# We are IntechOpen, the world's leading publisher of Open Access books Built by scientists, for scientists

**4,800**
Open access books available

**122,000**
International authors and editors

**135M**
Downloads

Our authors are among the

**154**
Countries delivered to

**TOP 1%**
most cited scientists

**12.2%**
Contributors from top 500 universities

CLARIVATE ANALYTICS BOOK CITATION INDEX INDEXED

WEB OF SCIENCE™

Selection of our books indexed in the Book Citation Index in Web of Science™ Core Collection (BKCI)

## Interested in publishing with us?
## Contact book.department@intechopen.com

Numbers displayed above are based on latest data collected.
For more information visit www.intechopen.com

# 3

# The High-speed Flywheel Energy Storage System

Stanisław Piróg, Marcin Baszyński and Tomasz Siostrzonek
*University of Science and Technology*
*Poland*

## 1. Introduction

At the present level of technology the electricity generation has already ceased to be a problem. However, years are passing by under the slogan of seeking for methods of effective energy storage. The energy storage method shall be feasible and environmentally safe. That's why the methods, once regarded as inefficient, are recently taken into consideration. The development in materials technology (carbon fibre, semiconductors, etc.) brought back the concept of a flywheel. This idea has been applied to high-speed flywheel energy storage.

## 2. Electromechanical energy storage using a flywheel

A flywheel energy storage system converts electrical energy supplied from DC or three-phase AC power source into kinetic energy of a spinning mass or converts kinetic energy of a spinning mass into electrical energy.
The moment of inertia of a hollow cylinder with outer radius $r_z$, and inner radius $r_w$ is:

$$J = \frac{1}{2}\pi h\rho\left(r_z^4 - r_w^4\right) \tag{1}$$

Maximum amount of kinetic energy stored in a rotating mass:

$$W_{k\max} = \frac{1}{2}J\omega_{\max}^2 = \frac{\pi}{4}h\rho\left(r_z^4 - r_w^4\right)\omega_{\max}^2 \tag{2}$$

where: $J$ – moment of inertia, $\omega$ – angular velocity.
The force acting on a segment of spinning hoop (Fig. 1) is:

$$dF_r = dm \cdot \frac{v^2}{r} = \rho \cdot h \cdot d\varphi \cdot dr \cdot v \tag{3}$$

where: $\rho$ – density of the hoop material, $h$ – height, $r$ – radius, $v$ – peripheral velocity, $\varphi$ – angle, $F$ – force, $m$ – mass.
The net force acting in the direction of axis $x$, resulting from elementary forces $dF_r$, is:

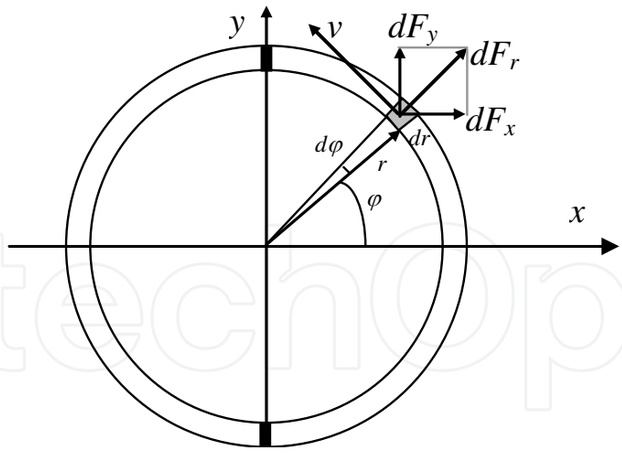


Fig. 1. Forces acting on the segment of a rotating hoop

$$F_x = 2\int_0^{\frac{\pi}{2}} dF_r \cos\varphi \cdot d\varphi = 2\rho \cdot h \cdot dr \cdot v^2 \int_0^{\frac{\pi}{2}} \cos\varphi \cdot d\varphi = 2\rho \cdot h \cdot dr \cdot v \tag{4}$$

Bursting stress (in the hoop cross sections shaded in Fig. 1):

$$\sigma_r = \frac{F_x}{2 \cdot h \cdot dr} = \frac{2\rho \cdot h \cdot dr \cdot v^2}{2 \cdot h \cdot dr} = \rho \cdot v^2 \tag{5}$$

Hence, the maximum allowable peripheral velocity for a material with the density $\rho$ and allowable tensile stress $R_e = \sigma_{r\max}$:

$$v_{\max}^2 = \frac{R_e}{\rho} \tag{6}$$

Maximum rotational velocity of a flywheel depends on the allowable peripheral velocity at its surface (6):

$$\omega_{\max}^2 = \frac{v_{\max}^2}{r_z^2} = \frac{R_e}{r_z^2 \rho} \tag{7}$$

Substituting (7) into (2) we have:

$$W_{k\max} = \frac{\pi}{4} h\rho\left(r_z^4 - r_w^4\right)\frac{R_e}{r_z^2\rho} = \pi\left(r_z^2 - r_w^2\right)h\frac{\left(r_z^2 + r_w^2\right)R_e}{r_z^2\rho} = V\left(1 + \left(\frac{r_w}{r_z}\right)^2\right) \tag{8}$$

Hence can be found the flywheel mass:

$$m = \pi h\left(r_z^2 - r_w^2\right)\rho = \frac{4W_{k\max}}{R_e} \cdot \frac{1}{1 + \left(\frac{r_w}{r_z}\right)^2}\rho \tag{9}$$

In order to minimize the flywheel mass it shall be made in the form of a thin-walled hollow cylinder.
From relation (9) the ratio of maximum stored energy to the flywheel mass is:

$$\frac{W_{k\max}}{m} = \frac{W_{k\max}}{\rho V} = \frac{R_e}{\rho} \cdot \frac{1 + \left(\frac{r_w}{r_z}\right)^2}{4} \tag{10}$$

For $r_z \approx r_w$ relation (10) reduces to the form of:

$$\frac{W_{k\max}}{m} \approx \frac{R_e}{2\rho} = \frac{v_{\max}^2}{2} \tag{11}$$

As follows from (11), a light structure (a large amount of energy per unit of mass) can be achieved using a material with possible low density $\rho$ and high tensile strength $R_e$. Materials that meet these requirements are composites (Kevlar, carbon fibre, glass fibre in combination with a filler) or composite bandage (in order to improve stiffness) on a ring of a light metal, e.g. aluminium.

| | Density $\rho$ [kg/m$^3$] | Strength Re [GPa] | $v_{\max}$ [m/s] | W/m [MJ/kg] |
|---|---|---|---|---|
| Steel | $7.8 \cdot 10^3$ | 1.8 | 480.4 | 0.23 |
| Titanium | $4.5 \cdot 10^3$ | 1.2 | 516 | 0.27 |
| Composite glass fibre | $2.0 \cdot 10^3$ | 1.6 | 894.4 | 0.80 |
| Composite carbon fibre | $1.5 \cdot 10^3$ | 2.4 | 1256 | 1.60 |

Table 1. Parameters of typical flywheel materials

A flywheel of a larger energy per unit of mass and the given outer radius $r_z$, chosen for constructional reasons, has to rotate with a higher peripheral velocity (11) and, consequently, with a higher angular velocity (7).
Since in this case peripheral velocities of high-speed rotors are exceeding the speed of sound, the rotor should be enclosed in a hermetic vacuum chamber. In consequence, the energy store structure - and particularly bearings, become complicated (due to vacuum maintained in inside the enclosure should be used magnetic bearings and a system stabilizing the rotor axle position in space The flywheel, integrated with the electric machine, should rotate without a contact with motionless parts (magnetic levitation). Magnetic bearings should be made of permanent magnets (high efficiency is required) while an electromagnetic system should only assist them to a certain extent and stabilize the axle position. Due to a required very high efficiency, the flywheel shall be driven by a permanent magnet motor installed inside the enclosure. Vacuum inside the enclosure prevents exchange of heat between the FES components and causes problems with heat removal from windings of the electric machine operated as a motor or generator. An advantage of vacuum is lack of losses caused by the rotor friction in air (at peripheral velocities of 700-1000m/s) and noiseless operation.

The electric machine must be controlled by a power electronic system enabling its operation as a motor or generator and adjusting electric power parameters alternately to the needs of the accelerated spinning mass or electrical loads (or an electric network) supplied from FES. If the energy storage system is operated as an autonomous energy source (isolated operation) it must be provided with a power electronic system that prohibits propagation of load unbalance (the output voltage double-frequency ripple component) to the flywheel torque.
The amount of energy stored in FES is proportional to the square of angular velocity. It means that at the 1/3 of maximum velocity remains only ca. 10% of maximum energy. The energy store should be therefore operated within the speed range from 1/3 to maximum speed. The voltage at the electric machine winding changes with the ratio 1:3, and the power electronic system shall be designed to tolerate such changes. in order to minimize losses (conduction losses in semiconductor devices) the maximum voltage applied to electric machine should be possibly high (up to 1000V).
The design of an energy storage system that meets up-to-date requirements is an interdisciplinary and complex engineering task that requires the use of the-state-of-the art technologies and materials. The energy storage system can be applied to:

- Power quality improvement systems to compensate active power peaks and limit their impact on power supply network and reduce peak loads. Required are: a large stored energy (of the order of hundreds MJ) and large instantaneous power that enables discharging during a tens of seconds.
- Standby power supplies to backup or start other power sources (a motor-generator set or switching to another network) for particularly important and sensitive processes.
- Systems for storage and controlled release of energy produced by alternative autonomous electric power sources, like photovoltaic or wind power plants. In such systems store energy in time when there is no demand from electricity users. A flywheel energy storage system intended for supporting alternative autonomous sources shall exhibit very high energy efficiency (due to the necessity of long accumulation time) and three-phase output with possibility for unbalanced load at constant frequency (50 Hz) and constant rms voltage magnitude. The amount of stored energy is ca. 5÷10 MJ.
- Limiting wind farms power fluctuations by means of a dynamic accumulation of peak power generated during high-wind periods and release it during low-wind periods.
- Accumulation (storage) of energy recovered from regenerative braking of intermittently started and stopped (or reversing) large-power drives (e.g. rolling mills and winders) or energy recovered from discharging large electromagnets.
- Elevators in buildings with intensive traffic flow ("intelligent building"). An elevator equipped with an energy storage system will consume energy solely to compensate losses.
- Large industrial plants (large-power flywheel energy storage systems) in order to mitigate voltage fluctuations, power supply back-up during supply systems switching, and power quality improvement by means of peak loading and unloading reduction. Reduction of peak active power will result in reduced transmission losses and enable the use of more economical installations (smaller cross-sectional areas, transformer powers, etc.), smaller peak contracted power.
- Urban buses. Flywheel energy storage systems designed for mobile applications with relatively small energy stored (6÷10 MJ) and suitable for charging and discharging with large powers (100÷150 kW) can be utilized in urban buses (charged at bus stops).

- Urban and suburban electric transportation systems and hybrid vehicles (internal combustion engine, generator, electric motor), flywheel energy storage systems can absorb kinetic energy of a braking vehicle and reuse it during travel.

## 3. Technical requirements for flywheel energy storage systems

- High efficiency.
- Small mass and volume.
- Reliability, durability and safety.
- Capability for operation in a three-phase power network or autonomous operation with unbalanced load.
- Large short-duration power (capability for quick charging and discharging).

## 4. Electric machine for the flywheel energy storage purposes

Flywheel energy storage systems can utilize all types of AC three-phase machines. The choice of the machine type is determine by the energy storage application and particularly by expected duration of energy storage. In energy storage systems with expected long duration of energy storage idle losses should be radically limited. Idle losses in systems with long duration of energy storage should be radically limited. Such systems can utilize asynchronous induction machines or synchronous machines. During energy charging or discharging a small amount of energy is needed for the machine excitation (power losses in the field winding resistance in a synchronous machine or losses due to the magnetizing (reactive) component in an induction machine). In energy storage systems intended for relatively short duration storage, permanent magnet machines (synchronous or brushless) can be used. In flywheel energy storage systems with a high rotational speed and, consequently, high frequency of the fundamental component of the machine voltage, the difficulty lies in correct shaping of sinusoidal current waveform obtained by means of PWM modulation. In such a case a correct power supply of a brushless DC machine can be more easily achieved. Permanent magnet machines require no additional energy for excitation but certain small losses occur in them due to currents induced in conducting parts by variable magnetic field of rotating magnets. These losses can be reduced employing brushless coreless machines. Such machines have very small winding inductance and in order to achieve a continuous current they require additional external reactors when supplied from PWM modulated inverters.

## 5. Examples of flywheel energy storage applications

In an autonomous system with alternative electric energy source (Fig. 2a) the energy store supplies loads if loss of supply from a base power source occurs. The energy storage can be used in uninterruptible power supply systems (UPSs) of selected loads (Fig. 2b). Upon voltage loss or decrease in the line voltage magnitude a load and energy storage system are instantaneously disconnected (by means of thyristor switches) from the supply line and energy store turns to the generator mode, thereby powering sensitive (critical) loads Another application of an energy storage system is stabilization of supply voltage (or limitation of peak currents in a supply line) of loads characterized with fast-changing, short-duration loading far exceeding the average load.

(a) Support of alternative autonomous electric power sources (PV – photovoltaic cell)

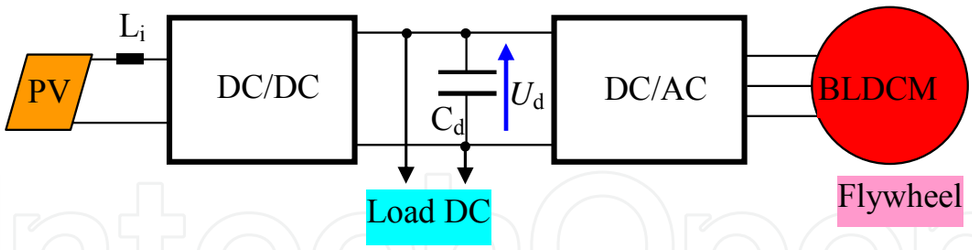


(b) Uninterruptible power supply of selected AC loads

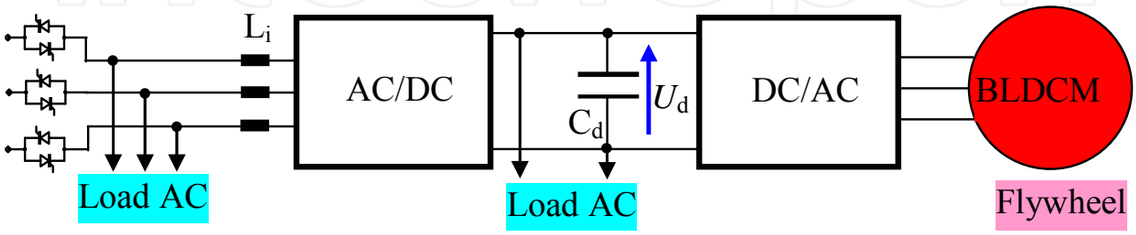


(c) Compensation of active power load fluctuations and voltage stabilization

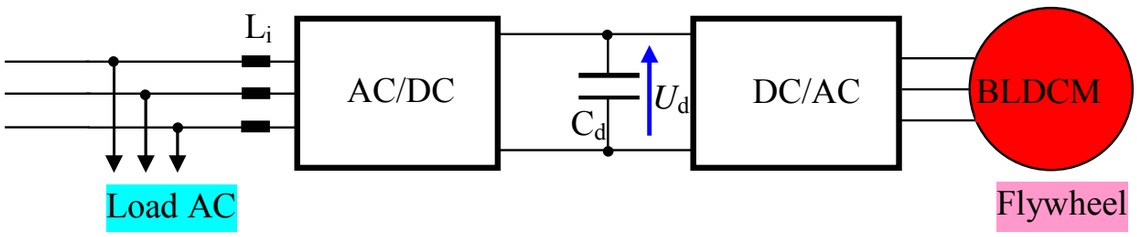


Fig. 2. Examples of spinning energy storage applications; AC/DC, DC/AC – power electronic converters, BLDCPM – electric machine (Brushless D.C. Permanent Magnet Motor)

## 6. Controlling energy release from a flywheel energy storage system

The amount of energy stored in a rotating mass is proportional to the angular velocity squared. It means that energy store can be effectively utilized within the range from maximum angular velocity ($W_{max}$) to 1/3 of angular velocity (1/9 $W_{max}$). There are several solutions for limiting the maximum power of energy release from (or supplied to) the energy store.

Figure 3 shows the relative energy ($W/W_m$) and power ($P/P_m$) vs. relative angular velocity ($\omega/\omega_m$). Line (1) is the characteristic of a storage system operated within the velocity range $(0.5\div1)\omega_{max}$ with limited power. The consequence of the power limitation is the necessity for limiting the current maximum value according to relation $I_{d\max} = P_{\max} / U_m$ (curve 3). Line (2) represents the power change for operation with the current maximum value determined by the straight line (4).

Another control method consists in operation with constant maximum power within the angular velocity range $(0.5\div1)\omega_{max}$. Characteristics of the storage system controlled employing this method is shown in Fig. 4. A boundary of the control method can be set at a lower velocity; this results in limiting maximum power to a lower value.

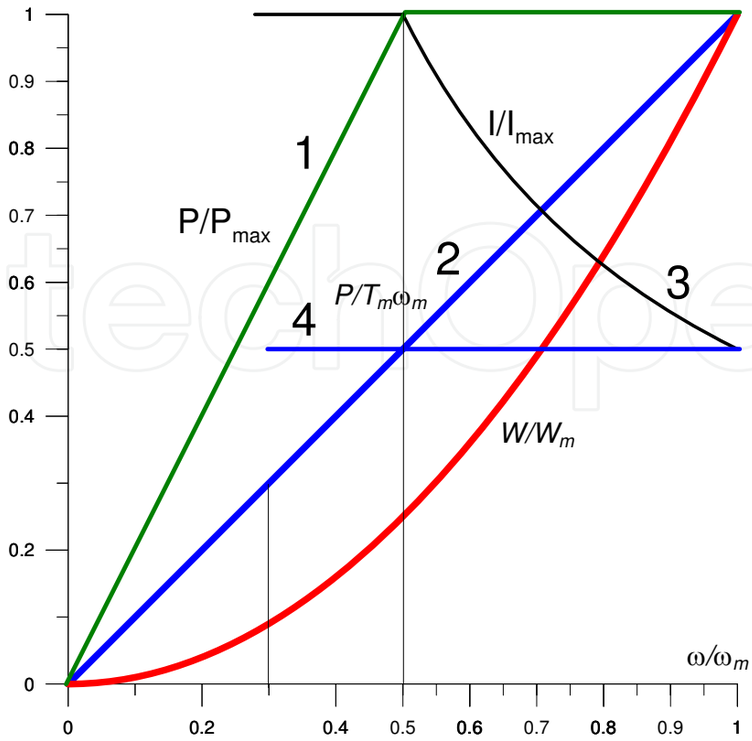


Fig. 3. Characteristic of a energy storage system with $P_{max}=f(\omega)$

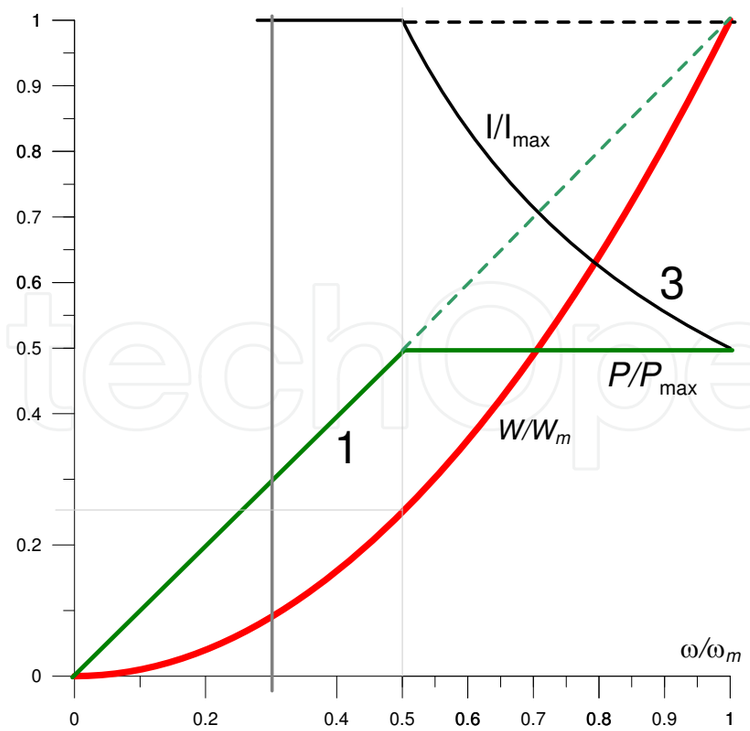


Fig. 4. Characteristic of a energy storage system with $P/P_{max}=const$ for $\omega>\omega_{max}/2$

It should be borne in mind that energy of 1kWh (3.6 MJ) is equivalent to potential energy of the mass 1000 kg at the height of 367 m, i.e. the release the amount of energy (equivalent to that consumed by a 100 W bulb during 10 hours) required to throw a 1-ton car to the height of 367 m ($3.6 \cdot 10^6$[J] =1000[kg]·9.81[m/s$^2$]$h$ hence $h$ =367[m]; air friction and the car and ground deformations are not taken into account).

## 7. Permanent magnet motors

Permanent magnet motors combine features of classical DC separately excited motors with advantages of an induction motor drive. They are manufactured in many structural variations with respect to both the permanent magnets arrangement and the method of their fixing, as well as the motor applications (permanent magnets in the stator or rotor). In terms of the current and the back electromotive force waveforms, permanent magnet machines can be categorized into two types:

- Permanent Magnet Synchronous Motor (PMSM),
- Brushless Permanent Magnet DC Motors (BLDCM, BLDC, BLPMDCM).

Permanent magnet synchronous motors (*PMSM*) exhibit properties similar to those of synchronous AC machines. They are characterized by:

- sinusoidal distribution of magnetic flux in the air gap,
- sinusoidal phase currents,
- sinusoidal back electromotive force (*BEMF*).

In a brushless permanent machine the back electromotive force has a trapezoidal waveform and the required current waveform has the form of rectangular, alternating sign pulses. Idealized relations between the back electromotive force and phase currents are shown in figure 5.

In order to provide a constant torque the machine should be supplied in such a manner that the instantaneous power value remains constant (in figure 5 the instantaneous power waveform in each phase is indicated green). This requirement is met for rectangular phase currents Duration of both the positive and negative pulse is T/3, time-interval between pulses is T/6, and phase-shift between phases is T/3. During each time interval T/6 the current is conducted simultaneously only in two phases. The motor instantaneous power is the sum of powers generated in two phases. The electromagnetic torque is the quotient of the instantaneous power and the motor angular velocity. At constant angular velocity the torque is constant only if the instantaneous power is constant.

A brushless DC permanent magnet motor cannot, as a machine, be supplied without supplementary equipment, thus its integral components are:

- a power electronic converter that provides power supply of appropriate phase windings depending on the rotor position,
- a controller stabilizing the current depending on the required torque (Fig. 6).

## 8. Bipolar PWM of an inverter supplying a brushless DC permanent magnet motor

The pulse-width modulated voltage-source inverter, supplying a brushless DC permanent magnet motor enables shaping the required phase currents waveform by means of the supply voltage control.

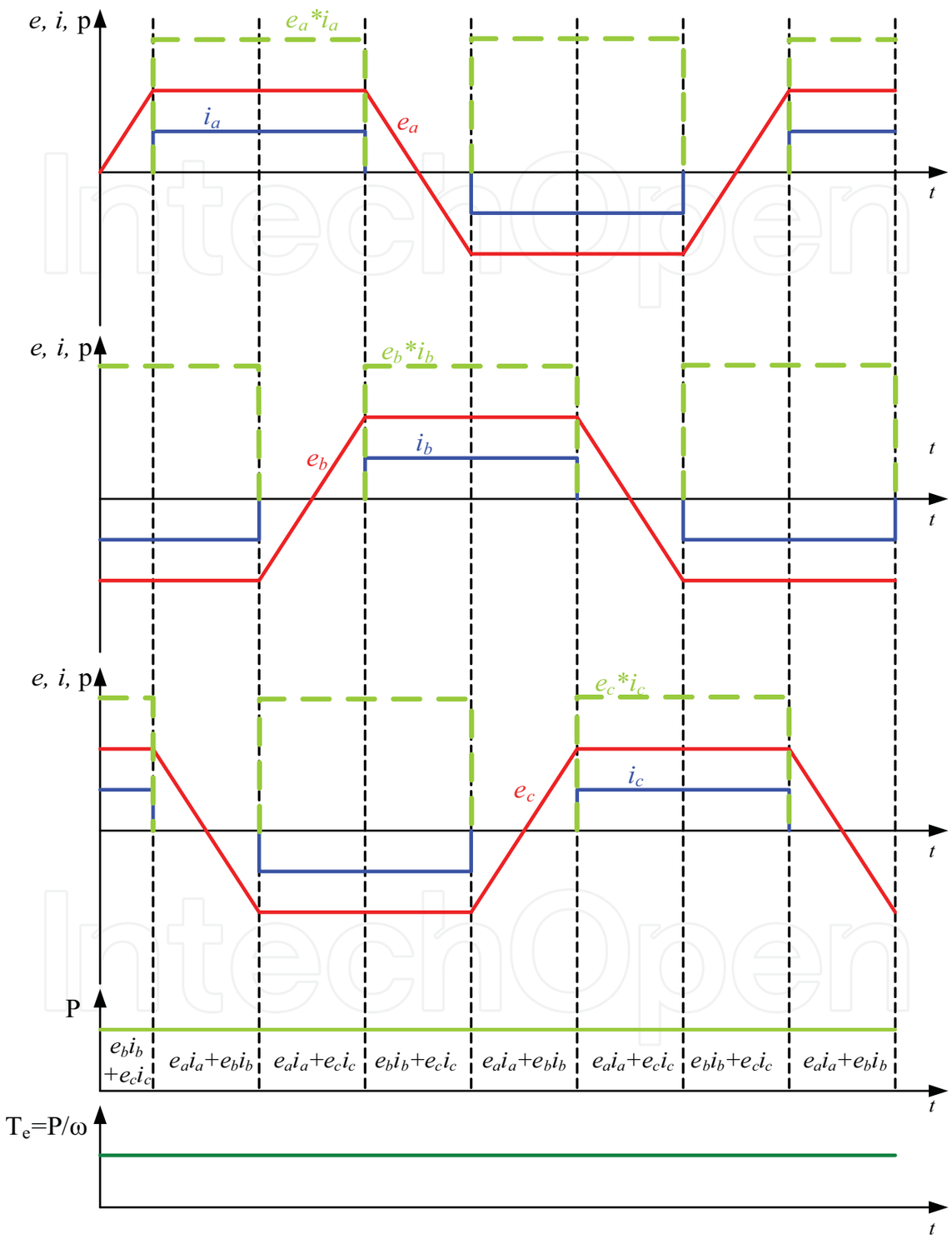


Fig. 5. Desired waveforms of electromotive force, phase currents, instantaneous power and electromagnetic torque

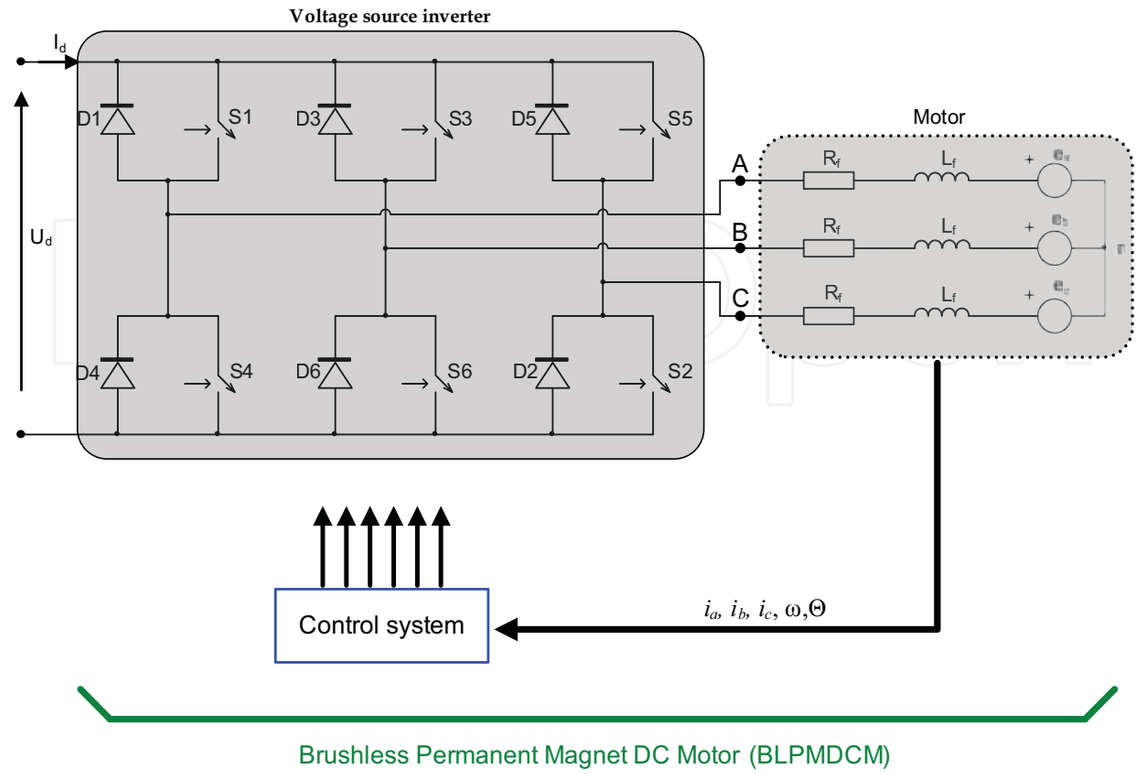


Fig. 6. A brushless permanent magnet DC motor supplied from a voltage source inverter with control system

Where this type of control is employed, only two switches are chopper controlled during the time interval of duration T/6. The sequence of switching is shown in figure 7. The inverter is controlled in the same manner as a single-phase inverter. The switches pairs, e.g. S1 and S6, are switched during the time interval equal T/6. The current flows through two phases A and B connected in series. After elapse of time equal T/6 switch S6 stops conducting and switch S2 is turned on to conduct (chopper controlled) together with the switch S1. Phase A is still connected to the DC voltage source positive terminal, phase B is being connected to its negative terminal. The current flows in phases A and C connected in series. Switch S1 is active during time period T/3 During each time interval with duration T/6 one of the phases is disconnected from both terminals of the DC voltage source, switches are switched specifically at T/6 intervals. At each time-instant the converter operates as a single-phase inverter and can be analysed as such. The inverter configurations with individual switches turned on are shown in figure 8.

## 9. Torque control of brushless permanent magnet DC machine

Figure 9 shows phase currents ($i_a$, $i_b$, $i_c$), their modules ($|i_a|$, $|i_b|$, $|i_c|$), the sum of the modules ($\Sigma|i|$) and torque ($T_e$). Apart from the fast-changing torque component resulting from finite time of semiconductor devices PWM switching, also torque ripple occurs due to the current commutation between the motor phase windings. Thus in each 1/6 of the period a noticeable disturbance occurs in the torque waveform.

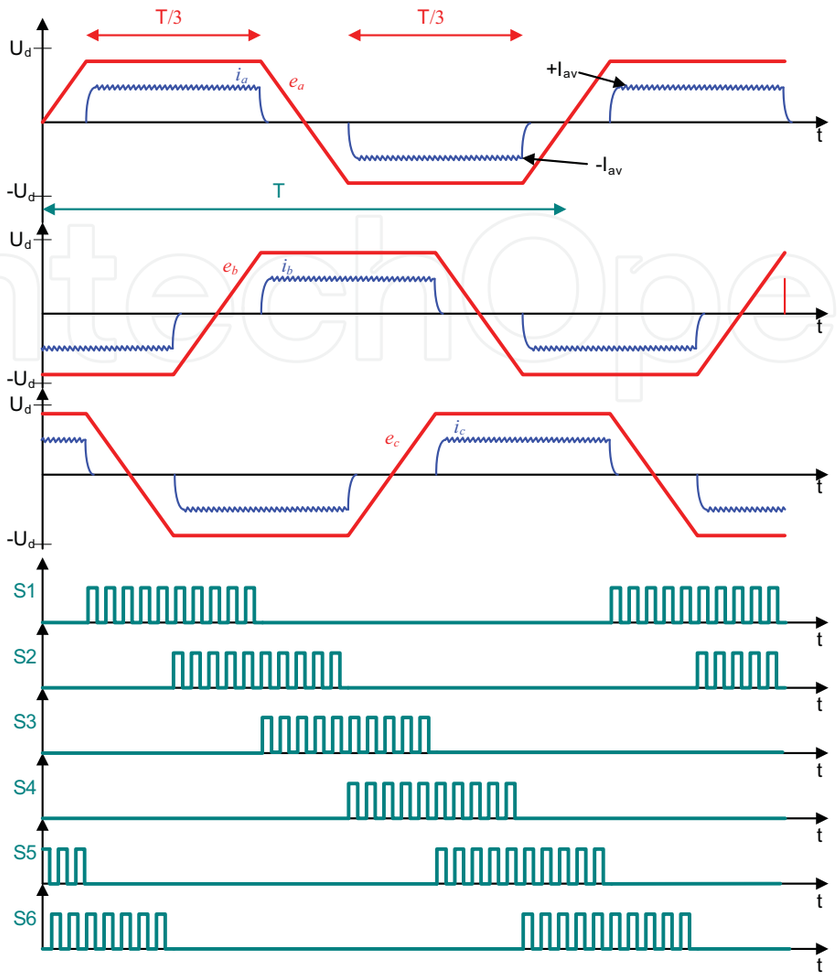


Fig. 7. Bipolar pulse width modulation: phase currents and switch control pulses

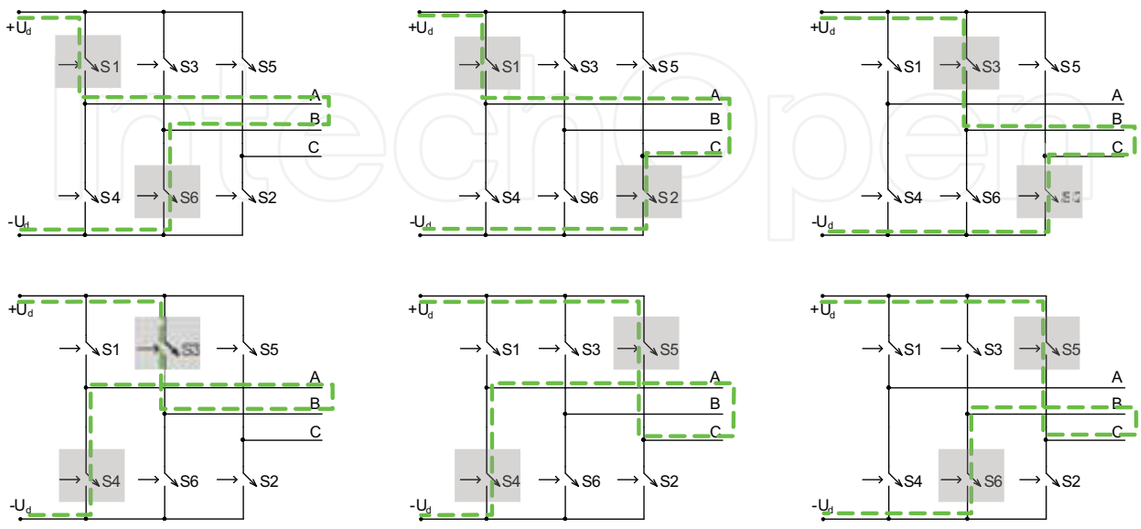


Fig. 8. Bipolar pulse width modulation: the sequence of switching

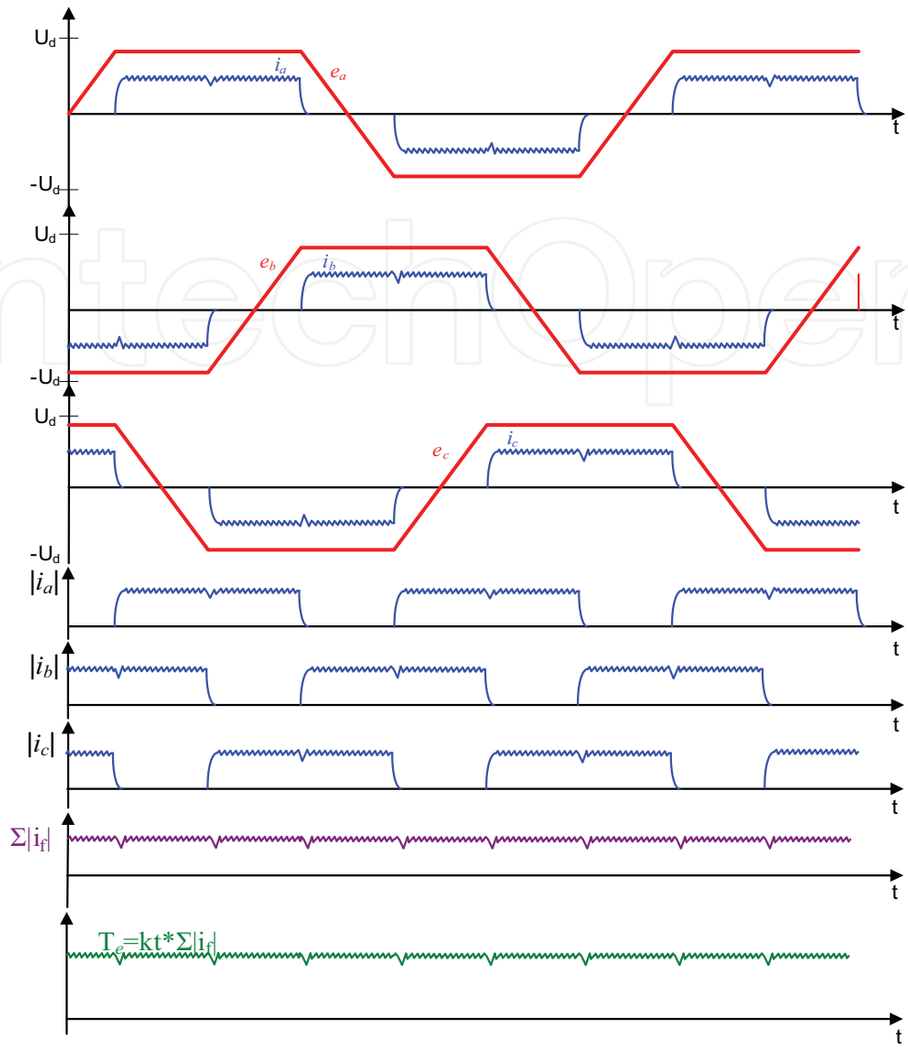


Fig. 9. Actual waveforms of phase currents, their modules and electromagnetic torque

The brushless machine torque is controlled by means of the phase currents control. The control is achieved, similarly as in a classical shunt DC machine, by modulation of fixed frequency pulses width by the output signal of a PI current controller. The feedback signal should be proportional to the actual value of the DC source current module. It can be obtained in two ways:

- measuring the module of the converter input current (DC source current) (Fig. 10), or
- measuring phase currents; the feedback signal is proportional to the sum of the load rectified phase currents (Fig. 11).

A drawback of the first solution is an additional inductance (of the sensor and its connections) connected between the capacitor and semiconductor devices. The inverter should be supplied from a voltage source and the incorporated inductance changes the source character during transient states. This inductance is the source of overvoltages occurring across semiconductor devices that require overvoltage protection in the form of RC snubber circuits to absorb overvoltage energy. These additional components increase both the system complexity and power losses in the converter.

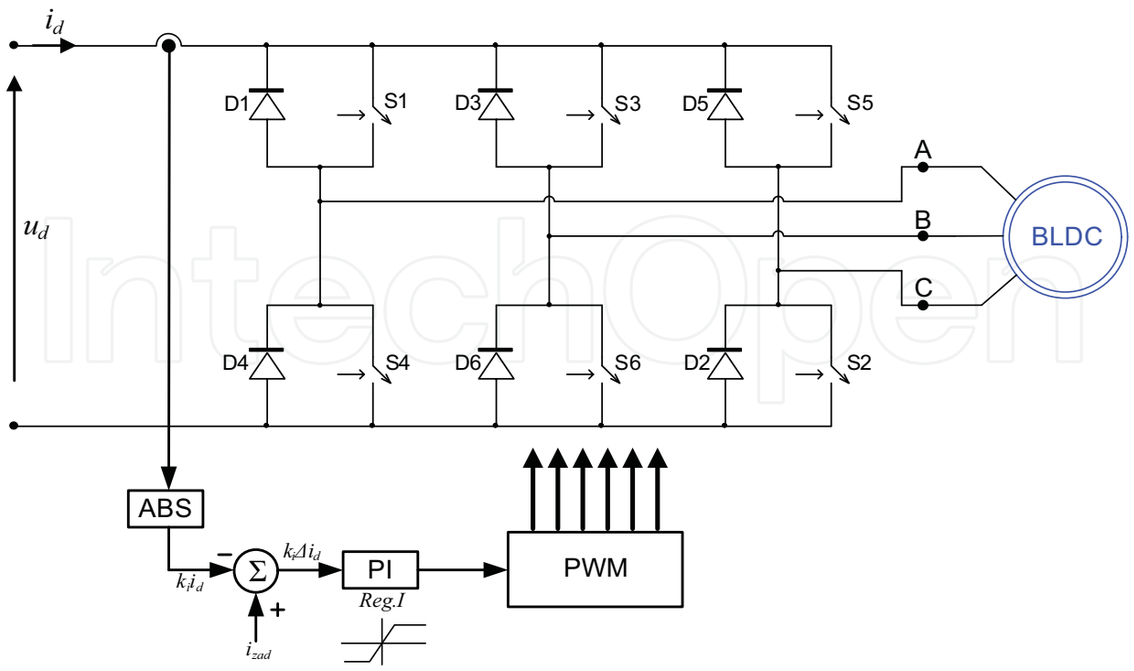


Fig. 10. Measurement of the inverter input current

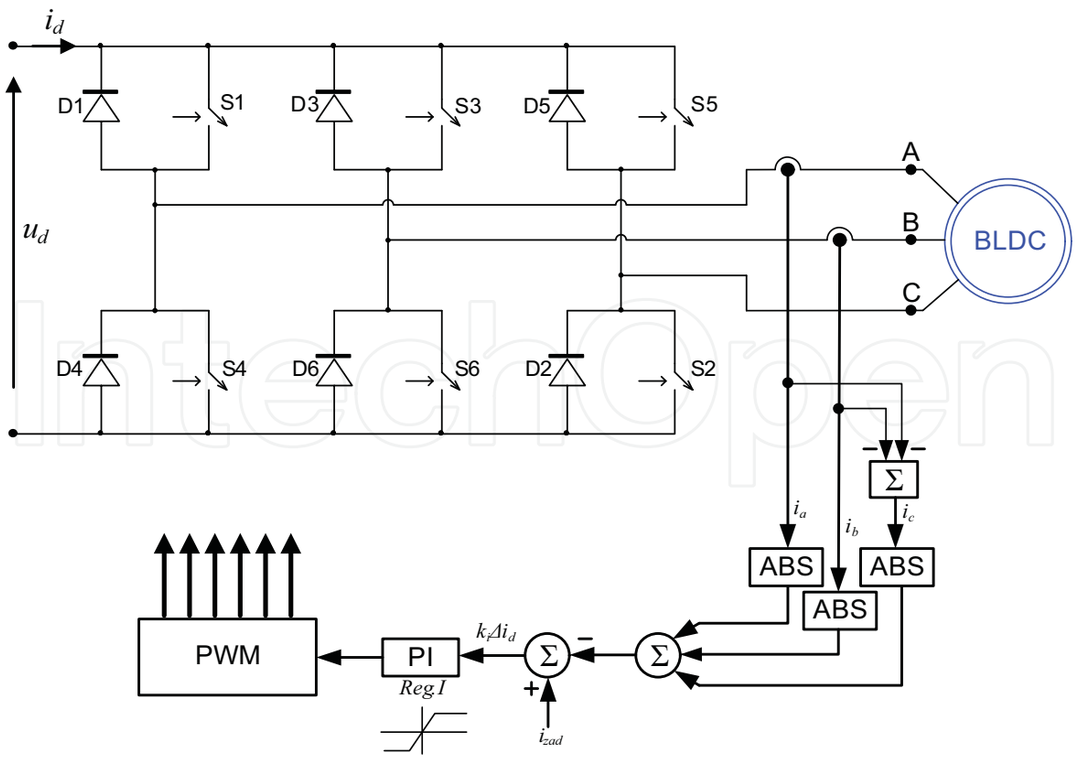


Fig. 11. The feedback signal circuit utilizing the phase currents measurement

Apart from current components from controlled switches, also the currents of backward diodes occur in the DC source current. These currents, flowing in the direction opposite to the switches current, result from the magnetic field energy stored in the machine windings and transferred back to the DC source. The phase current value depends on both these components. Therefore, in order to obtain the feedback signal, the absolute value of the signal proportional to the measured DC source current has to be taken.
The second way the feedback signal can be obtained is the measurement of phase currents. Since $i_a+i_b+i_c=0$ it is sufficient to use transducers in the load two phases. The signal proportional to the DC source current is obtained by summing the absolute values of phase currents (Fig. 11). The error signal is the difference between the DC current reference and the actual source current, reconstructed from the measured phase currents. In the pulse width modulation a high-frequency triangle carrier signal is compared with the current controller output signal. The current controller output signal limit is proportional to the phase-to-phase peak voltage value. That way are generated control pulses of fixed frequency and modulated width to control the inverter transistors switching.

## 10. Determining the rotor poles position relative to stator windings

Figure 12 shows the cross section of a brushless permanent magnet DC motor. The motor is assumed to have a single pole-pair rotor while the stator winding has three pole-pairs. Figure 13 shows waveforms of the current and back electromotive force in phase A depending on the mutual positions of characteristic points. The analysis starts at the instant when point K coincides with point $z_1$. At his time the magnet N-pole begins overlapping the stator pole denoted by a. The back electromotive force (BEMF) increases linearly until the stator pole is completely overlapped by the magnet N-pole. This takes T/6. Then, the magnetic flux increases linearly during T/3 thus the back electromotive force is constant. The rectangular waveform of the current in phase A is shaped by means of chopper control.

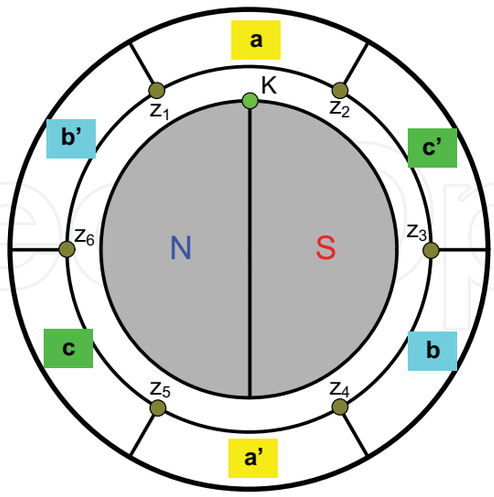


Fig. 12. The cross section of a BLDCM motor

Since point K coincides with $z_4$ the back electromotive force decreases linearly until point K is in the position where N-pole begins overlapping the stator pole denoted a'. Between the point $z_5$ and $z_1$ the back electromotive force is constant and negative.

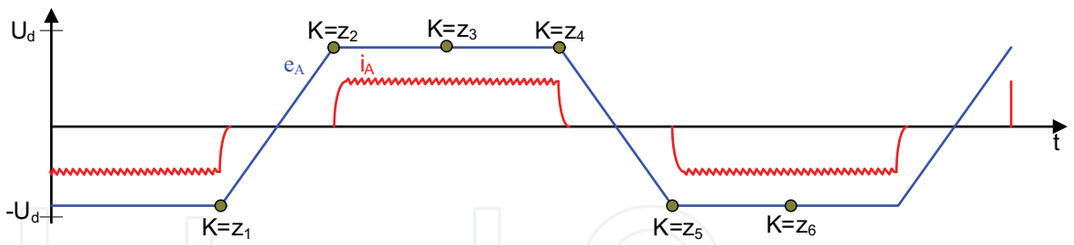


Fig. 13. Waveforms of the current and back electromotive force in one phase depending on the permanent magnet poles position

In motors with trapezoidal BEMF it is essential that voltage switching on or off to a given winding is synchronized with the rotor position relative to this winding axis.

## 11. AC/DC converter

A unity input power factor control of a three-phase step-up converter is feasible in the rotating co-ordinate frame because in this system the source frequency quantities are represented by constant values. The diagram of the rectifier connection to a supply network is shown in figure 1. Since $X_L$>>$R$, the resistances of reactors are disregarded in the diagram.

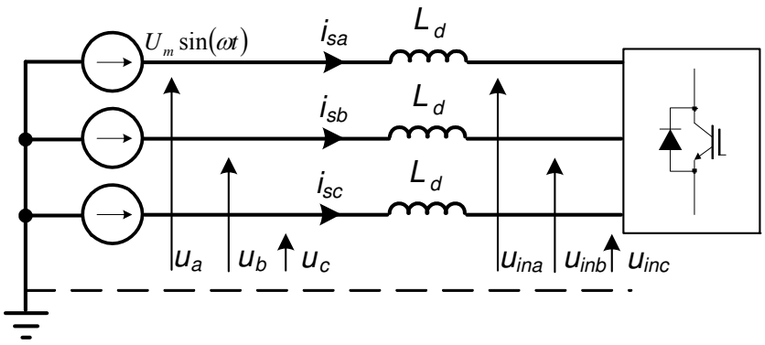


Fig. 14. Diagram of the rectifier connection to a supply network

The following designations are used the diagram of figure 1: $i_{sn}$– phase currents, $u_{sn}$– the supply line phase-to-neutral voltages, $u_{inn}$– the converter output voltage (where $n$= $a$, $b$, $c$). The phase currents, according to the diagram, are described by equation (12).

$$u_{sn} - u_{inn} = L\frac{di_{sn}}{dt} \tag{12}$$

Converting the equation (12) into the rotating reference frame $dq$ we obtain equation (13).

$$\boldsymbol{u}_{sdq} - \boldsymbol{u}_{indq} = \Delta\boldsymbol{u}_{dq} = L_d\frac{d\boldsymbol{i}_{sdq}}{dt} + j\omega L_d\boldsymbol{i}_{sdq} \tag{13}$$

Decomposing the equation (12) into $dq$ components we obtain (14).

$$u_{ind} = u_{sd} - \Delta u_d = u_{sd} - (L_d\frac{di_{sd}}{dt} - \omega L_d i_{sq}) \tag{14}$$

$$u_{inq} = u_{sq} - \Delta u_q = u_{sq} - (L_d \frac{di_{sq}}{dt} - \omega L_d i_{sd}) \tag{15}$$

Equations (14) and (15) describe the converter input voltages. Inserting the required line current values into these equations we can determine the output voltage waveforms forcing the required current. The components $L_d(di_{sdq}/dt)$ represent the converter dynamic states (load switching or changes in the load parameters). Assuming the control system comprises only proportional terms we obtain from equations (14) and (15) relationships describing the control system (16) and (17).

$$u_{ind} = u_{sd} - (K_R \Delta i_{sd} - K_d \Delta i_{sq}) = u_{sd} - [K_R(i_{sdr} - i_{sd}) - K_d(i_{sqr} - i_{sq})] \tag{16}$$

$$u_{inq} = u_{sq} - (K_R \Delta i_{sq} - K_q \Delta i_{sd}) = u_{sq} - [K_R(i_{sqr} - i_{sq}) - K_q(i_{sdr} - i_{sd})] \tag{17}$$

Figure 15 shows block diagram of the control system and the power circuit. The following designations are used in the diagram: *TP* – switch-on delay units (blanking time),

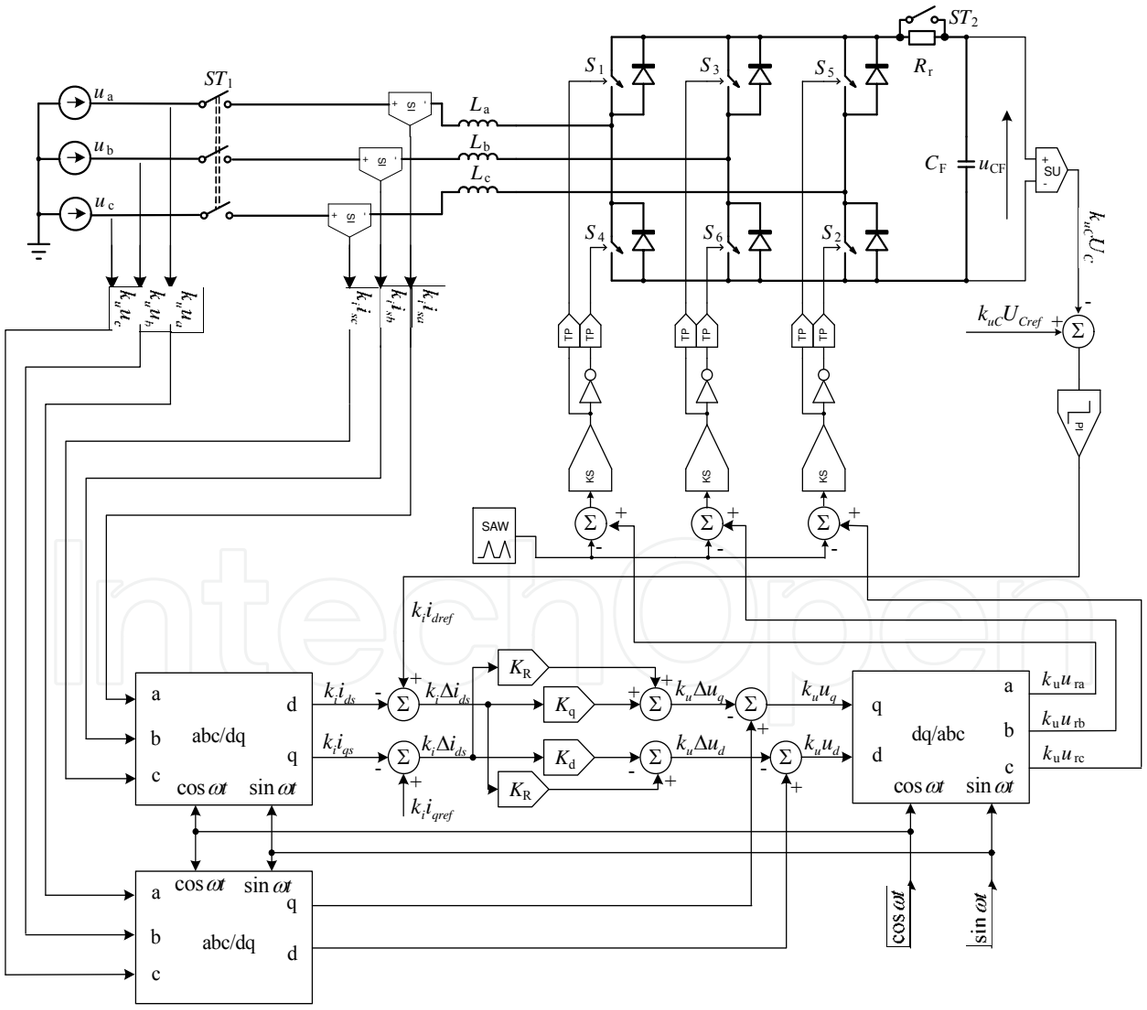


Fig. 15. Block diagram of the control system and the power circuit

*PI* – proportional-integral controller, *KS*- sign comparator, *SAW*- triangle wave generator, $K_R$, $K_d$, $K_q$- proportional terms, *ST*- contactors, $R_a$, $R_b$, $R_c$ - resistors limiting the capacitor charging current, $\Sigma$- adder.
The control circuit of diagram 15 employs transformation from the thee-phase system to the rotating co-ordinate system (abc→dq), described by equation (12).

$$\begin{bmatrix} v_d \\ v_q \end{bmatrix} = \begin{bmatrix} \cos\omega t & \sin\omega t \\ -\sin\omega t & \cos\omega t \end{bmatrix} \begin{bmatrix} v_a \\ \frac{1}{\sqrt{3}}(v_b - v_c) \end{bmatrix} \tag{18}$$

Where:

$$\begin{cases} v_a = V_m \cos\omega t \\ v_b = V_m \cos(\omega t - \frac{2}{3}\pi) \\ v_c = V_m \cos(\omega t + \frac{2}{3}\pi) \end{cases} \tag{19}$$

### 11.1 Synchronization circuit

In order to determine the transformation abc→dq it is necessary to generate functions $\cos\omega t$ and $\sin\omega t$, as follows from equation (18), such that the function $\cos\omega t$ will correspond (i.e. be cophasal) to $v_a=V_m\cos\omega t$. In practical solutions various methods for generating the $\cos\omega t$ and $\sin\omega t$ functions are employed, e.g. synchronization with a single, selected phase (normally *a*) employing a single-phase PLL loop. The advantage of this method is an easy implementation in digital technique. Microprocessor systems employ an external, specialized device performing the functions of a phase-locked loop, connected with a microprocessor port dedicated for counting external events. Therefore the CPU workload due to generating the $\cos\omega t$ and $\sin\omega t$ functions is reduced to minimum. A drawback of this method is the generated function is related to only one phase of the synchronizing signal and the system does not control the other phases. In the event of a disturbance starting in phase *c* (a phase jump in the synchronizing voltage caused by switching a large active power load) the control system will respond with large delay. In order to protect the converter from effects of a phase jump the synchronization circuit should control all phases of the synchronizing voltage. Substituting equations (19) describing the three-phase synchronizing voltage into equation (18), the transformation abc→dq takes the form (20).

$$\begin{bmatrix} v_d \\ v_q \end{bmatrix} = \begin{bmatrix} V_m(\cos^2\omega t + \sin^2\omega t) \\ V_m(-\sin\omega t\cos\omega t + \sin\omega t\cos\omega t) \end{bmatrix} = \begin{bmatrix} V_m \\ 0 \end{bmatrix} \tag{20}$$

It follows from equation (20) that if the functions $\cos\omega t$ and $\sin\omega t$ are generated correctly ($\cos\omega t$ is cophasal with voltage in phase *a*), the component in axis *d* equals the amplitude of the synchronizing voltage, whereas the component *q* is zero. This property of the abc→dq transformation is employed in the design of the three-phase synchronization circuit depicted in figure 16.
The following designations are used in figure 16: *PI*- proportional-integral controller, *VCO*- voltage controlled square-wave generator. The *PI* controller input signal is the instantaneous value of the *q*-axis component of abc→dq transformation. The controller tunes the *VCO* oscillator, whose output signal controls the $\cos\omega t$ and $\sin\omega t$ generation circuit. The controller

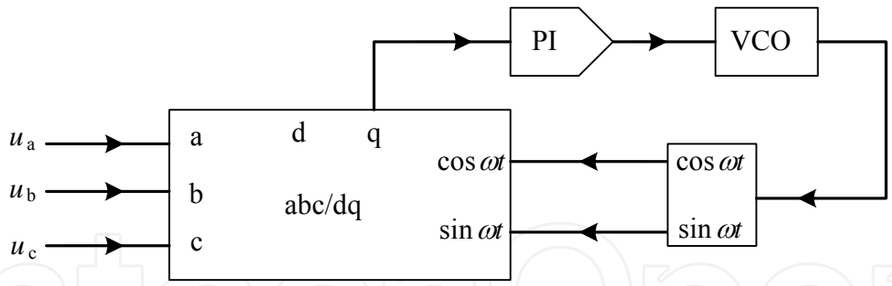


Fig. 16. Block diagram of the synchronization circuit

connected to the *q*-axis controls the *PI* controller error to zero (the value *q*-axis component equals zero) what means that, according to equation (4), the generated cos$\omega t$ signal is cophasal with synchronizing voltage $u_a$. The control circuit shall attain the state in which the *q*-axis component value is zero. This condition ($q$= 0) is satisfied in two cases:

1. The generated function cos$\omega t$ is cophasal with the synchronizing voltage $u_a$. This case is described by equation (20). Figure 17 shows oscillograms of the synchronizing voltage ($u_a$, $u_b$, $u_c$) and the generated function cos$\omega t$. The simulation waveforms are computed using a model of the system implemented in FPGA.

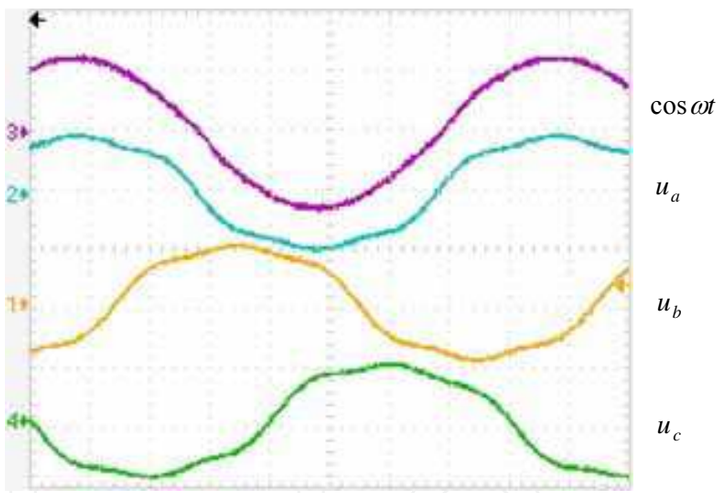


Fig. 17. The synchronizing voltage waveforms and the generated function cos$\omega t$

2. The generated function cos$\omega t$ is phase-shifted in with respect to the synchronizing voltage $u_a$ by $\pi$. The transformation abc→dq then takes the form described by equation (21).

$$\begin{bmatrix} v_d \\ v_q \end{bmatrix} = \begin{bmatrix} -\cos\omega t & -\sin\omega t \\ \sin\omega t & -\cos\omega t \end{bmatrix} \begin{bmatrix} v_a \\ \frac{1}{\sqrt{3}}(v_b - v_c) \end{bmatrix} \tag{21}$$

Substituting (19) to equation (21) yields (22).

$$\begin{bmatrix} v_d \\ v_q \end{bmatrix} = \begin{bmatrix} -V_m(\cos^2\omega t + \sin^2\omega t) \\ V_m(\sin\omega t\cos\omega t - \sin\omega t\cos\omega t) \end{bmatrix} = \begin{bmatrix} -V_m \\ 0 \end{bmatrix} \tag{22}$$

The phase shift of $\cos\omega t$ function (by $\pi$) with respect to the voltage $u_a$ results in erroneous power relationships in the converter operation and is, therefore, inadmissible. This case is illustrated in figure 18 which shows the simulation waveforms computed using the system model.

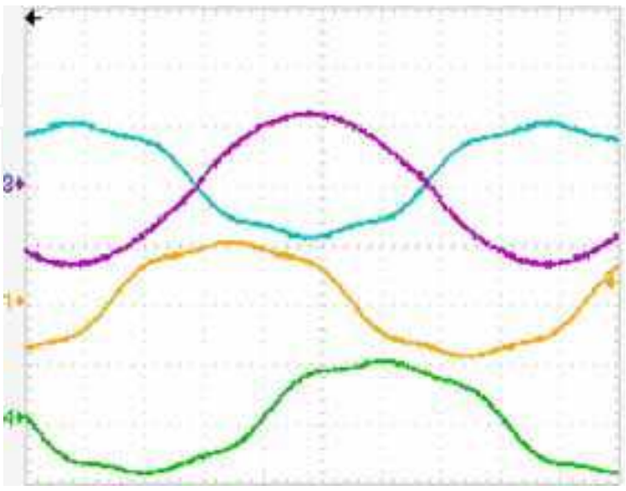


Fig. 18. The synchronizing voltage waveforms and the generated function $\cos\omega t$

The operating point of the synchronizing circuit from figure 16 (case *1* or *2*) is determined by the initial phase of synchronizing voltages at the instant of the converter start. In order to prevent a random selection of the operating point the synchronization circuit should be modified to enforce the system operation according to equation (20) (case*1*). Figure 19 shows two possible versions of the synchronizing circuit.

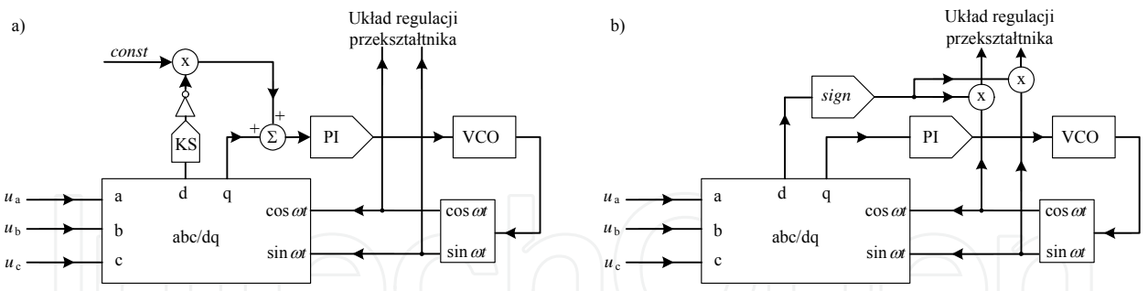


Fig. 19. Two versions of the synchronizing circuit enforcing the correct generation of $\cos\omega t$ function

The following designations are used in figure 19: *const* – a constant value, KS- sign comparator, *sgn*- sign of the signal (”1” if the signal is greater than zero, conversely ”-1”), other elements according to figure 14. If the *d*-axis component value (figure 19a) is less than zero, the case described by equation (22), the constant value *const* is added to the instantaneous value in axis *q* (the *PI* controller input error) therefore tuning the *VCO* oscillator, even when the *q*-axis component value is zero. When the control circuit attains the state in which the value of the *d*-axis component is greater than zero only the *q*-axis component is applied to the *PI* controller input (the controller error). In the circuit from figure 6b no modification is made to the synchronization circuit. The functions $\cos\omega t$ and

sin$\omega t$ are multiplied by the $d$-axis component sign prior to being applied to the converter control circuit. When the system operates correctly, i.e. according to equation (19), the functions cos$\omega t$ and sin$\omega t$ are directly applied to the converter control circuit. When the function cos$\omega t$ is phase-shifted with respect to the synchronizing voltage $u_a$ by $\pi$ (equation 22) the multiplication of cos$\omega t$ and sin$\omega t$ functions by the sign of $d$-axis component (”-1”) reverses their phases and the correct values of cos$\omega t$ and sin$\omega t$ functions are applied to the converter control circuit.
Figure 20 illustrates the synchronization circuit operation, the time graphs are recorded in the laboratory setup using the *SignalTap II Logic Analyzer* tool (a part of the *Quartus II* package).

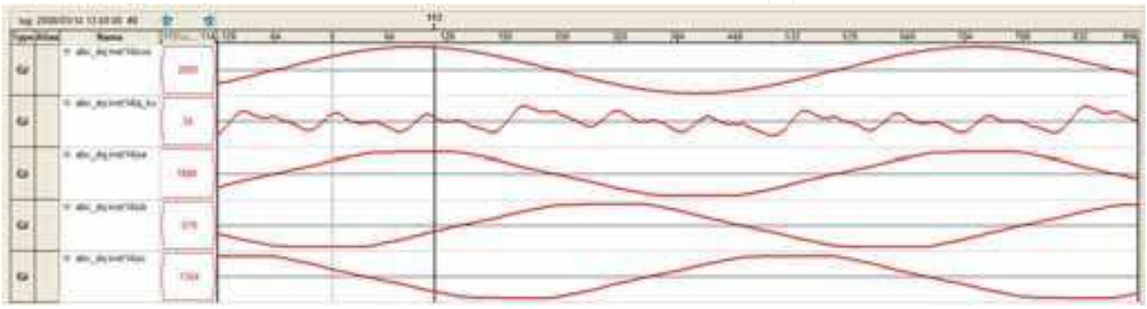

Fig. 20. The time graphs of cos$\omega t$ function, and the synchronizing voltages waveforms recorded in the experimental setup

Figure 20 shows the oscillograms of phase voltages $u_a$, $u_b$, $u_c$, the generated cos$\omega t$ function, and $q$-axis component (the controller in figure 19 input error). In the presented synchronizing circuit implementation all quantities are represented by eleven-bit numbers plus a sign bit. Instantaneous values of these quantities can vary within the range ±2047. According to equation (20) the values of $q$-axis component are equal zero if the synchronizing voltages are consistent with (19), i.e. are not distorted. Due to the power system voltage harmonic distortion with $1\pm6n$ harmonics (where $n$= 0, 1, 2…) the values recorded in axis $q$ are different from zero. These values were varying over the range ±98, what makes 4.78% of permissible range.

### 11.2 Investigation of the converter

Figure 21 shows the waveforms of the voltage and current in phase $A$ and the output voltage. As follows from figure 21 the proposed system allows obtaining the rectified voltage value higher than the phase voltage amplitude and forces a sinusoidal current, cophasal with the phase voltage. Figure 22 shows phasor diagrams for several selected parameters of the converter input voltage.
Figure 22a illustrates the case where the source current is cophasal with the supply voltage (cosφ= 1). In figure 22b the source current is lagging (cosφ≠ 1), i.e. a reactive component occurs in the source current. Diagrams in figures 22c and 22d are determined for the inverter mode operation (energy is fed back into the power system). As can be seen from the phasor diagrams, the source current fundamental harmonic cosφ (lagging or leading) can be influenced on by means of shaping the converter input voltage ($u_{in}$) and energy can be fed back into the power system. Example waveforms in figure 23 illustrate the transition from the rectifier to inverter mode of operation (energy is fed back into the power system).

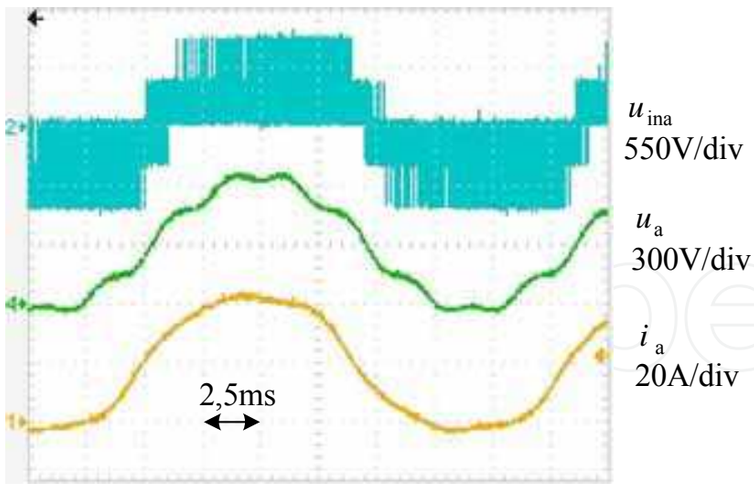


Fig. 21. The waveforms of the phase voltage and current $u_a$, $i_a$ and the input voltage $u_{ina}$ in phase *A*

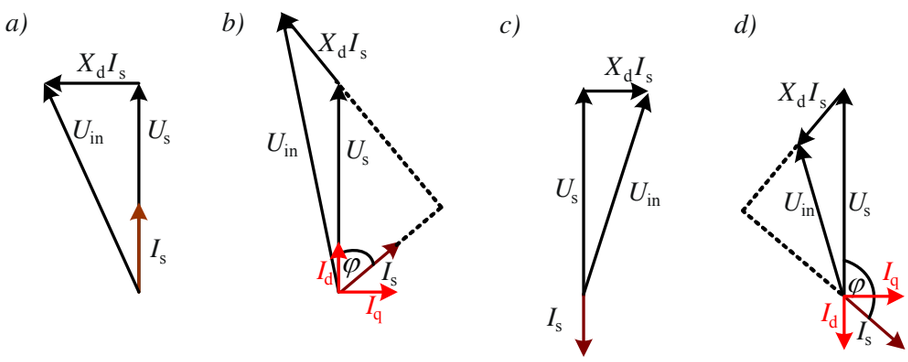


Fig. 22. Phasor diagrams for several selected parameters of the input voltage $U_{in}$ vector

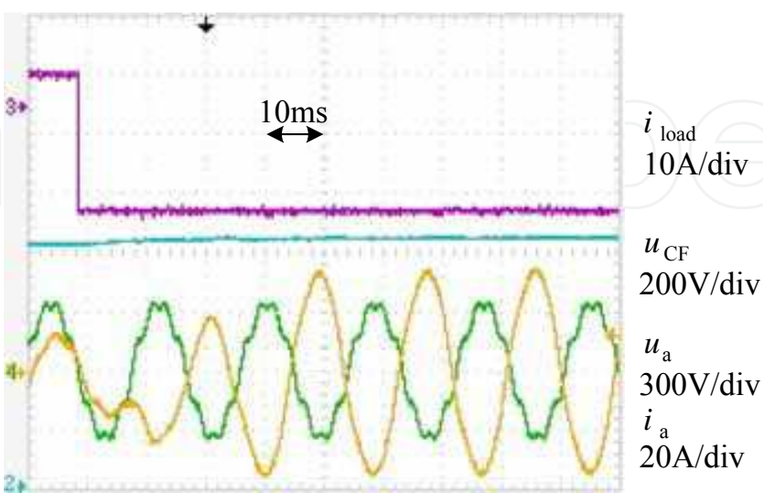


Fig. 23. The waveforms of the load current $i_{load}$, the output capacitor voltage $u_{CF}$, the voltage and current in phase *A*

As follows from figure 23, at the instant the load current direction is reversed, energy is transferred to the capacitor and its voltage $u_{CF}$ increases what, in turn, influences the source current phase shift in such a way that energy stored in the capacitor is fed back into power system.

The described converter is intended for co-operation with an inverter supplying a flywheel energy storage drive. Thus, in order to ensure constant operating conditions of the inverter-motor system, the rectifier should maintain the capacitor voltage at the set value irrespectively of the load current $i_{load}$ value and direction. Figures 14 and 15 show the waveforms recorded at a step change in the load current.

As can be seen from figure 23 at the instant of an increase in the load current the capacitor is discharging (the capacitor voltage decreases) and, consequently, the control system increases the phase current amplitude. Energy is supplied in an amount sufficient to compensate the capacitor voltage decrease resulting from the load current change and provide energy being drawn from the capacitor by the load. When the capacitor voltage becomes equal to the set voltage value of the phase current amplitude decreases to the value which ensures the capacitor voltage is maintained at the required level. In the event of an abrupt change in the load current a reactive component may occur in the phase current, as is shown in figure 25.

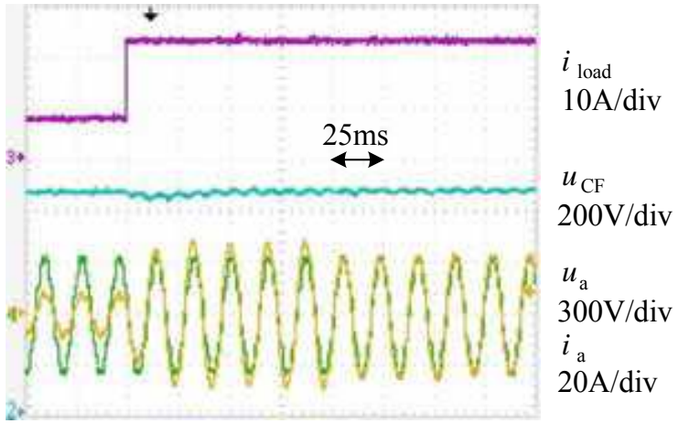


Fig. 24. The waveforms of the load current $i_{load}$, the output capacitor voltage $u_{CF}$, the voltage and current in phase *A* in response to a step-change in the load current

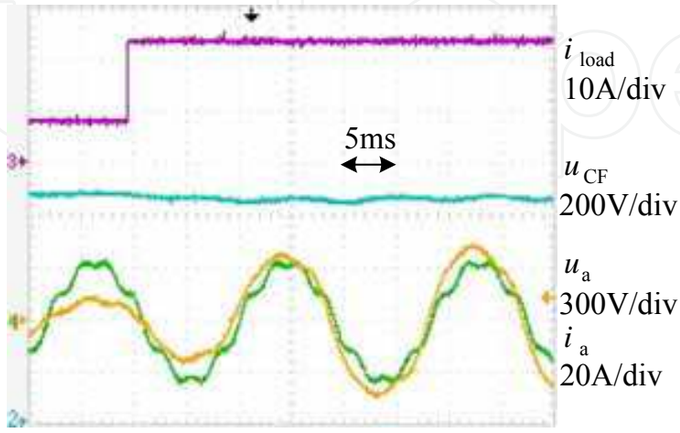


Fig. 25. The waveforms of the load current $i_{load}$, the output capacitor voltage $u_{CF}$, the voltage and current in phase *A*; a reactive component $i_q$ occurs in the source current

## 12. A flywheel energy storage drive control system

Figure 26 shows the diagram of power processing unit (power supply and inverters) and illustrates the mechanical structure of flywheel energy storage.

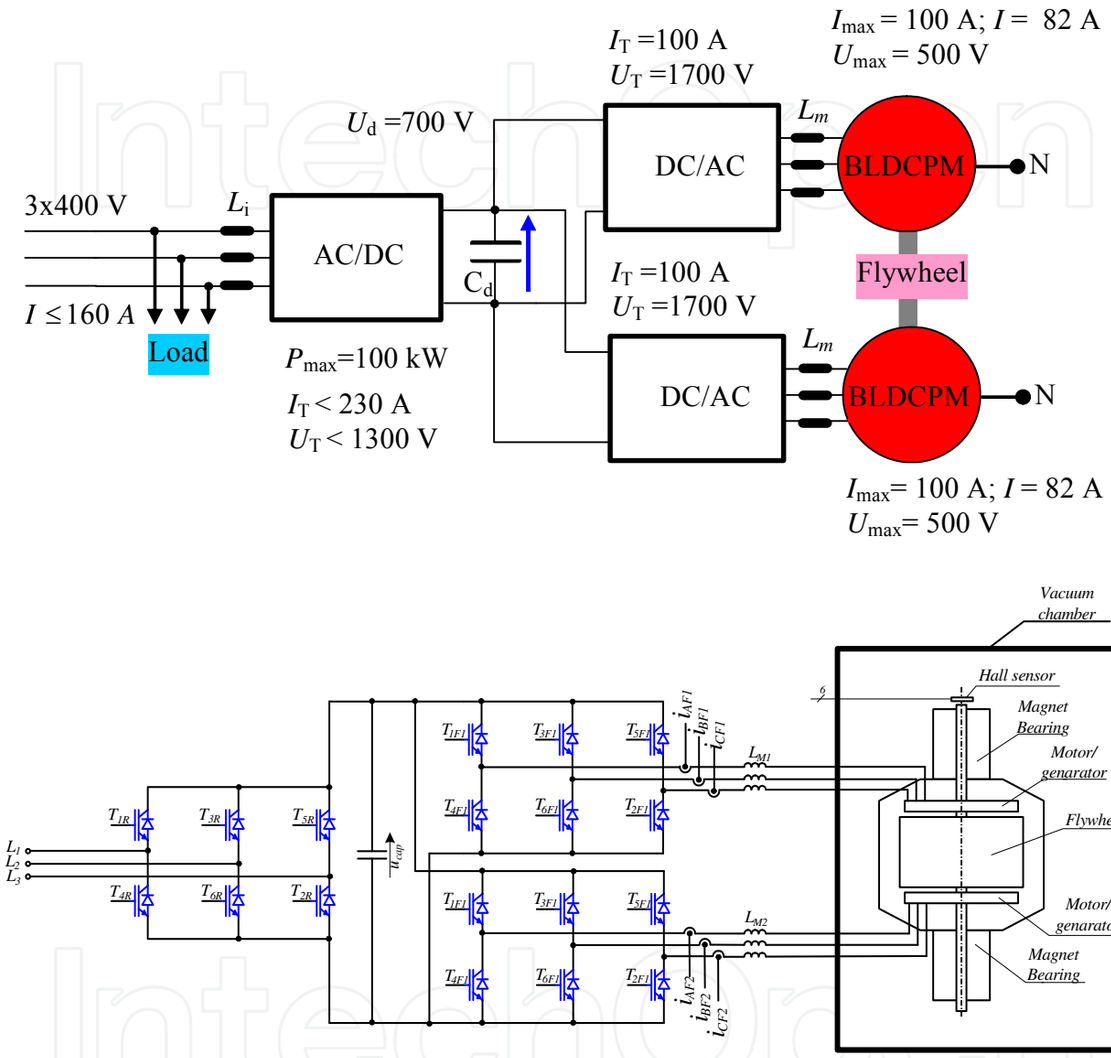


Fig. 26. High-speed flywheel energy storage: a – block diagram, b - power processing unit diagram

Two brushless permanent magnet DC motor are mounted on a common shaft. Magnetic bearings levitate the spinning mass in order to minimize the resistance to motion. The whole structure is enclosed in a vacuum chamber. The motor shaft positioning with respect to the stator is achieved by means of Hall sensors. they determine the instances of switching the inverter switches based on the actual rotor position relative to stator windings axes. The layout of magnets and windings of both motors is the same, thus the instants of commutation are determined by means of a single sensor, common for both motors. Each of the two FES motors is supplied from an independent inverter, of identical structure. Figure 28 shows diagram of the inverters control system.

The following symbols are used in figure 28: $H_A$, $H_B$, $H_C$ – the Hall encoder signals (the rotor position with respect to stator), *MUX* – multiplexer, *SAW* – symmetric sawtooth signal generator, $u_{cap}$ – DC link capacitor voltage, *ABS* – absolute value, *KS* – sign comparator, $i_{xFy}$ – (x= *A, B, C;* y= *1, 2*) the motors phase currents. The PWM generators sawtooth signals of both motors are shifted by *T/2*; consequently, the DC link capacitor current alternating component is doubled thereby reducing torque ripples at the FES shaft.
The converter controls the DC link capacitor voltage and if it drops below the predefined level the speed of 1/3 $\omega_{max}$ is set in the control system. The system turns from the motor mode to generator mode and the mechanical energy is converted into electrical energy. The capacitor voltage is also controlled during the converter start-up. The inverters remain blocked until the instant of a correct start-up of the line-side converter. The motor actual rotational speed is determined from the frequency of the Hall sensor signals. An algorithm for computing the frequency is described further below.

Fig. 27. Photograph of the FES mechanical structure

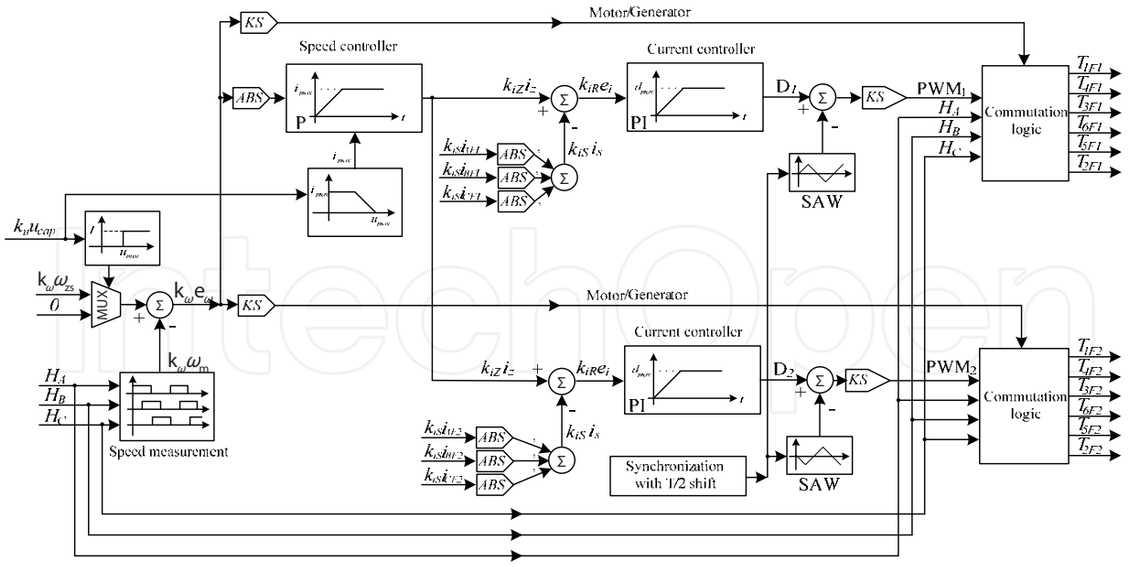


Fig. 28. The inverters' control system

The motors operate at a common shaft and rotate with same speed, therefore the inverters control system (Fig. 28) utilizes a single speed controller, common for both inverters. The speed controller output signal is proportional to the drive current reference value. In order to protect the system against an uncontrolled increase in the DC-link capacitor current the controller output signal is limited to a selected value proportional to the capacitor maximum voltage. This limitation determines the inverters' maximum current. When motors are operated in the generator mode the current limit level must be reduced depending on the instantaneous value of the DC-link capacitor voltage. When the energy recovered from the spinning mass (i.e. delivered to the capacitor) is larger than that supplied by the line-side converter to the supply line, the capacitor voltage increases. An increase in the capacitor voltage results in reduction of the speed controller output limit ($i_{max}$) and thereby the drive current limiting. If the capacitor voltage reaches its maximum permissible value the set current decreases to zero. The principle is illustrated in figure 29.

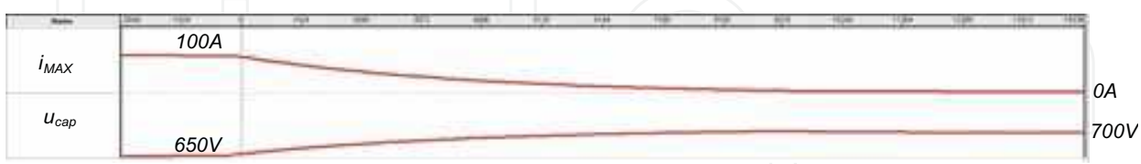


Fig. 29. The DC-link capacitor voltage (alternate component) and the speed controller output limitation (maximum permissible inverter current) versus time

Direction of energy transfer: power supply network ⇒ spinning energy storage (the inertial element ⇒ power supply network) is determined by the sign of the speed control error. If the set speed is lower than the actual rotation speed, the motors turn into generating mode (regenerative braking). In the alternate case the control error is grater than zero, the motors are accelerated or energy supplied from the power network compensates losses resulting from the resistance to motion. The control system automatically sets zero speed if the DC-link capacitor voltage is lower than 0.9 of its nominal value. This condition limits the supply

line current during the line-side converter start-up. The drive is started only if the capacitor is charged to $0.9U_N$ with delay of 2 seconds. In the event of voltage loss in the supply line, resulting in the capacitor voltage reduction, the system automatically turns to the generator mode.

The speed controller output signal (the current reference) is compared with the sum of absolute values of the motors phase currents. The inverters' current error ($k_{iR}e_i$) is applied to the PI current controller. Each inverter is provided with an independent controller divided into two parallel components: the proportional and integral part. Both parts of the controller have their own limits. The controller integrator incorporates a limiter that prevents counting when the integer value reaches a predefined maximum level. A separate limitation at the controller output prevents reaching the output signal values that cannot be executed by the control circuit. This limitation results from PWM generators operation area range.

The block termed "Commutation Logic", shown on the diagram in figure 3 is responsible for correct switching of the inverters' transistors, depending on the permanent magnets position with respect to the stator windings. Time relations between the motor electromotive force ($e_A$, $e_B$, $e_C$), Hall sensors signals ($H_A$, $H_B$, $H_C$), transistor switches control pulses ($T_1$, $T_2 \div T_6$) and phase currents ($I_A$, $I_B$, $I_C$) are shown in figure 30 (Fig. 30a refers to the motor mode operation, Fig. 30b refers to the generator mode). As can be seen from figure 30, logic functions controlling the switches in the motor and generator mode operation are different (transistor gate control pulses are shifted by $T/2$). The "Commutation Logic" block structure is shown in Fig. 31 The "Pulse Blocking" input is employed for blocking all transistors during starting (until the capacitor voltage reaches $0.9U_N$) and to turn off the line-side converter upon detection of exceeding the current permissible value.

The position sensor shall change its logic state at the angular distance of $\pi/6$ from the motor phase voltage ($e_A$, $e_B$, $e_C$) zero crossing. The current flows always through windings in which maximum voltage value occurs (Fig. 30). Therefore, during a full revolution of the rotor each of the inverter's transistors conducts during $2\pi/3$ of the cycle and participates in two from the six allowable pairs: $T_1T_2$, $T_2T_3$, $T_3T_4$, $T_4T_5$, $T_5T_6$, $T_6T_1$. Since only two switches can conduct simultaneously, in order to minimize switching losses only one transistor of a pair is chopper controlled while the other is continuously turned on. To ensure uniform heating of a transistor module a transistor is continuously turned on during ½ of the conducting period, while during the other half it is chopper controlled. In figure 30 the transistor switching process is indicated by shaded area. Figure 31a depicts the rotor position sensor signals and transistors gate control pulses (the waveforms recorded in Quartus II programme using the *SignalTap II Logic Analyzer* tool). Figure 31b shows oscillogram of the phase current waveform and a transistor gate control pulses. From the principle of inverter operation it follows that conduction times (pulse duty factor) of all the inverter transistors are the same. The PWM generator module operates in a continuous manner; the commutation logic, shown in figure mb.6, is responsible for assignment of control signals to individual transistors (depending on the rotor position with respect to stator).

In this figure each transistors has assigned its individual control signal $PWM_x$ ($x$= *1, 2 … 6*), which is a logical function of the common control PWM and the position sensors pulses; the functions for both the motor and generator operation mode are listed in table 2. The separation of the common control and the use of an appropriate logical function allows limitation of transistors switching losses according to the idea illustrated in figures 30 and 31. Logical functions listed in table mb.1 and logical circuits from figure mb.6, are exclusively correct for the phase sequence shown in figure 30.

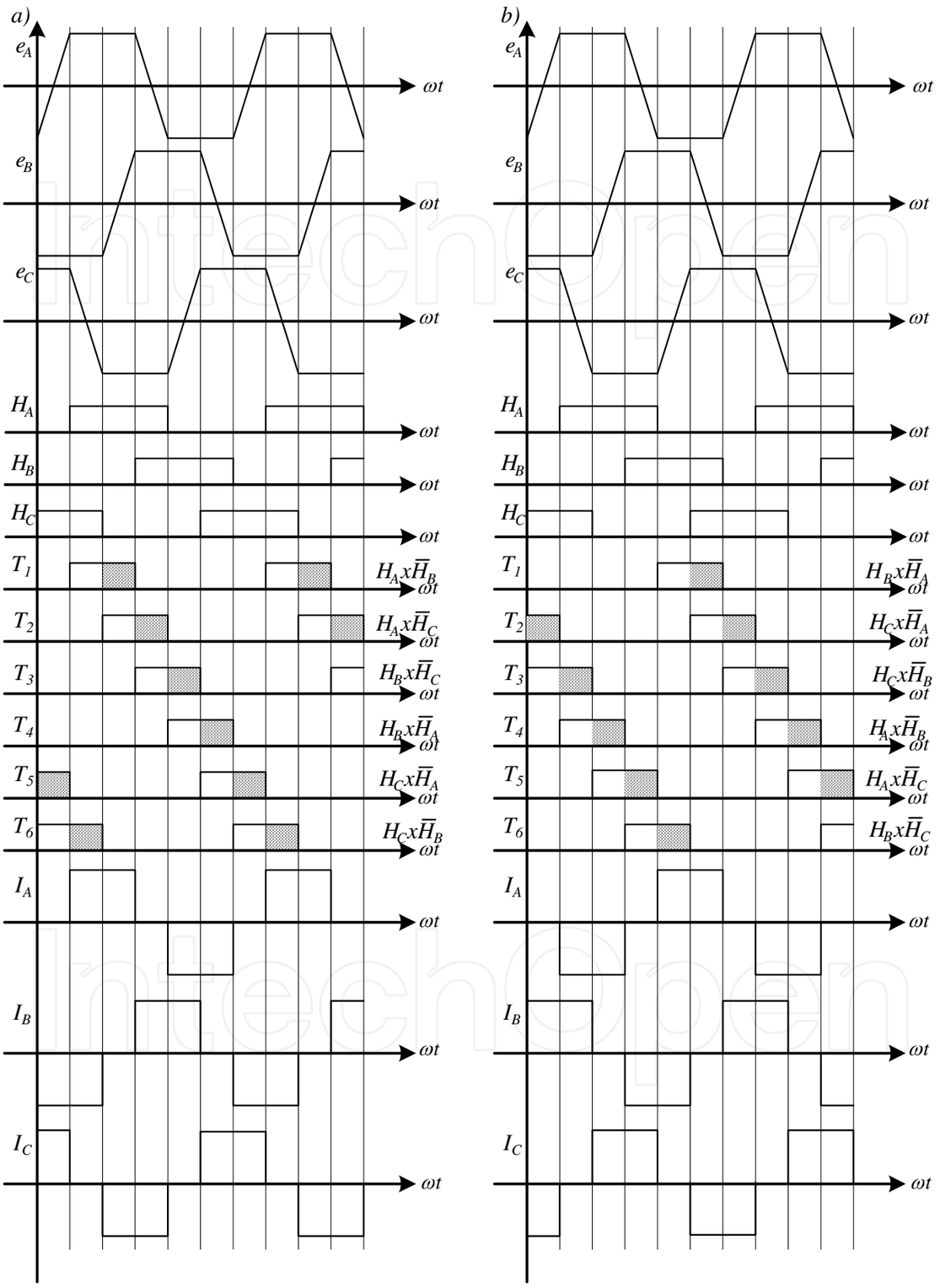


Fig. 30. Time relations between the motor back emf, phase currents, Hall sensors signals and the inverter switches control pulses; a) motor mode operation, b) generator mode operation

| Transistor | Motor | Generator |
|---|---|---|
| $T_1$= $PWM_1$ | PWM **or** ($H_A$ **and** $H_C$) | PWM **or** (**not**($H_A$) **and not**($H_C$)) |
| $T_2$= $PWM_2$ | PWM **or** (**not**($H_B$) **and not**($H_C$)) | PWM **or** ($H_B$ **and** $H_C$) |
| $T_3$= $PWM_3$ | PWM **or** ($H_A$ **and** $H_B$) | PWM **or** (**not**($H_A$) **and not**($H_B$)) |
| $T_4$= $PWM_4$ | PWM **or** (**not**($H_A$) **and not**($H_C$)) | PWM **or** ($H_A$ **and** $H_C$) |
| $T_5$= $PWM_5$ | PWM **or** ($H_B$ **and** $H_C$) | PWM **or** (**not**($H_B$) **and not**($H_C$)) |
| $T_6$= $PWM_6$ | PWM **or** (**not**($H_A$) **and not**($H_B$)) | PWM **or** ($H_A$ **and** $H_B$) |

Table 2. Logical functions for individual transistors control that allow minimizing switching losses

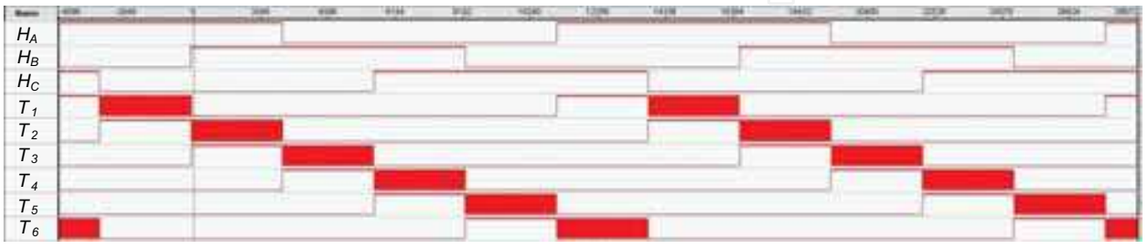


(a)


(b)

Fig. 31. a) Hall sensors signals and transistors gate control pulses; b) The motor phase current and transistor gate control pulses limiting switching losses

## 13. Speed measurement

The converter control system utilizes signals from rotor position sensors to detect which winding conducts current and, basing on their frequency, determines the speed of FES rotation. Using these signals the control algorithm can detect sensor failure (loss of

connection integrity) or locked rotor (because of e.g. bearings failure). If the logical state in all three signal lines (*HA, HB, HC*) does not change over a specified time interval, transistors' control pulses are blocked. This action protects the motor windings against overheating due to continuous current conduction. This blocking is independent of the speed measurement because the algorithm of digital speed measurement assumes a minimum determinable speed value, whereas the described failure detection method works correctly also at arbitrary low speeds. This is of particular importance when motors are started from zero speed.

The rotational speed measurement algorithm shall ensure the frequency of the output signal to be as high as possible and possible misalignment shall not impact the measurement result. Ideally, in a theoretical case, the position sensor pulses (*HA, HB, HC*) duty factor is 50%. If the Hall sensor axis is misaligned with respect to the motor shaft axis, or the sensor is not mounted perpendicularly to the shaft, the duty factor differs from the required value. The cycle of each of the three rotor position signals equals one period of the shaft revolution (for a two-pole pair motor) or a half of the revolution period - for a four-pole motor. Since the position sensor signals are shifted with respect to each other by 1/3 T, then determining the cycle of each signal (using either a rising or a falling edge) the measurement frequency is three times the rotation frequency (for a two-pole motor). The speed measurement frequency can be doubled determining the signal half-cycle (using both the rising and falling edge) and employing a supplementary register that stores the determined value of the preceding half-cycle. For each change in the sensor signal level the determined signal period is the sum of the current measurement result and that being stored in the supplementary register. The flowchart of the algorithm determining the sensor signal period is shown in figure 32.

The algorithm from figure mb.9 is executed in an infinite loop independently for each of three signals. Each step is executed on the rising edge of the clock signal (CLK) of known frequency. The internal counter representing the revolution period is incremented by one at the clock rising edge (the variable *Counter* in Fig. 32), next the level of the Hall sensor signal (*HA, HB, HC*) is checked. A change of logical state is interpreted as completing 1/2 of shaft revolution (1/4 for a motor with two pole-pairs). In such a case in supplementary registers (*R2_x, R1_x* where *x= A, B,* C) the current and the preceding value of counter is stored. The sum of the *R2_x, R1_x* registers values represents the rotational speed (frequency computed from completing a full revolution). If the sensor logical state did not change the counter value is checked and when it attains the specified maximum value it is assumed that the motor is stopped and its rotational speed is zero. In the case of a motor with two pole-pairs four supplementary registers are required, each of them stores the duration of the consecutive fourth part of a revolution. Figure 33 shows the waveforms recorded in Quartus II programme illustrating practical realization of the described algorithm. The variable *Counter* (Fig. 32) has not been taken into account in the practical realization, is function is fulfilled by the register *R1_x*.

The following symbols are used in figure 33:

$H_A$, $H_B$, $H_C$ – pulses from the rotor position sensor determining the current commutation instants (e.g. Hall sensor, sensorless method),

$G_A$, $G_B$, $G_C$ – signals of the rotor position sensors state change (pulse edge detection),

$G_I$ – the speed controller timing signal.

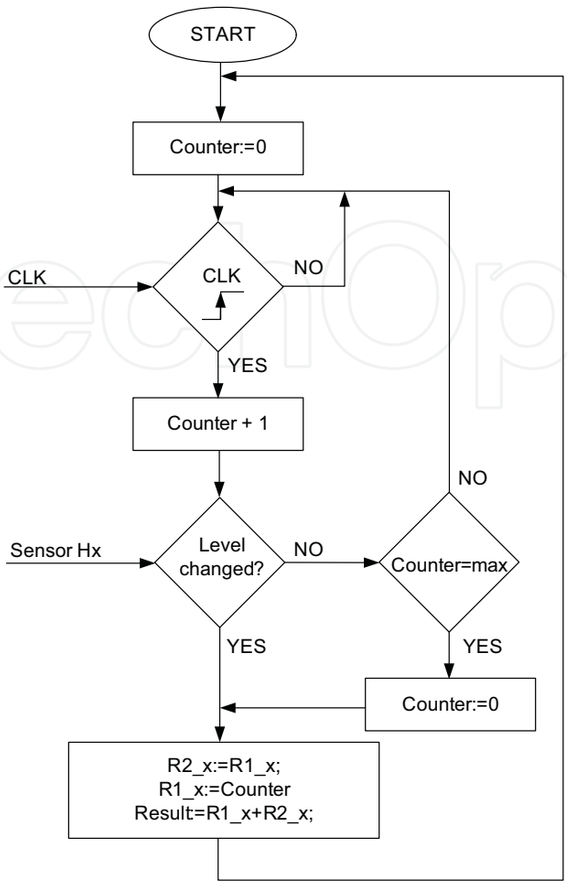


Fig. 32. Flowchart of the algorithm determining the frequency of a single Hall sensor signal

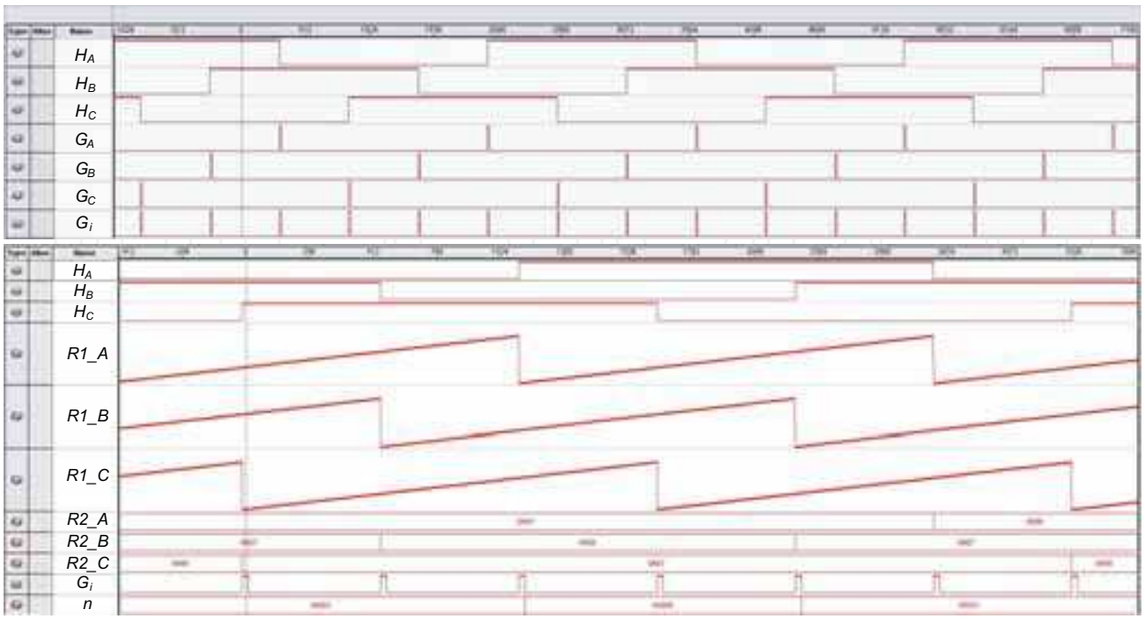


Fig. 33. The principle of the rotational speed measurement – a practical realization

Duration of the position sensor high and low states (a half of a revolution for a motor with one pair of poles or a quarter of a revolution for a motor with two pole-pairs) is timed by counting pulses of a known frequency between the consecutive pulses *Gx* (x= *A, B, C*). The rising edge *Gx* resets the *R1_x* (x= *A, B, C*) register counter (Fig. 27). Prior to resetting the *R1_x* register, its value is rewritten to the supplementary register *R2_x*. Knowing the reference signal frequency ($f_{CLK}$) and states of the registers *R1_x* and *R2_x* at falling edge of the *GI* signal we can determine the motor rotational speed from equation (23)

$$n = \frac{60 f_{CLK}}{R1\_x + R2\_x} \tag{23}$$

## 14. References


Aanstoos, T.A. Kajs, Brinkman J. P., Liu W.G., Ouroua H. P., Hayes A., Hearn R.J., Sarjeant C., Gill J., H.: *High voltage stator for a flywheel energy storage system*; Center for Electromech., Texas Univ., Austin, TX; Magnetics, IEEE Transactions on 04/25/2000 -04/28/2000, Jan 2001 Location: San Francisco, CA, USA

Acarnley P.P., Mecrow B. C., Burdess J. C., Fawcett J. N., Kelly J. G., Dickinson P. G.: *Design Principles for a Flywheel Energy Store for Road Vehicles*, IEEE Transactions on Industry Application vol. 32, no 6, 1996,

Akagi H., Sato H.: *Control and performance of a doubly-fed induction machine intended for a flywheel energy storage system*, IEEE Transactions on Power Electronics, Volume: 17 Issue: 1, Jan 2002,

Curtiss, D.H. Mongeau, P.P. Puterbaugh, R.L.: *Advanced composite flywheel structural design for a pulsed disk alternator*; Kaman Electromagnetics Corp., Hudson, MA; Magnetics, IEEE Transactions on 04/20/1994 -04/24/1994, 20-24 Apr 1994 San Diego, CA, USA.

Davies T. A., Jefferson C. M.: *Wind-power flywheel integration* Dept. of Eng., Bristol Polytech*:* Energy Conversion Engineering Conference, 1989. IECEC-89. Proceedings of the 24th Intersociety 08/06/1989 -08/11/1989, 6-11 Aug 1989 Washington, DC, USA; page(s): 2071-2076 vol. 4.

Davies, T.S. Larsen, N. *A: Regenerative drive for incorporating flywheel energy storage into wind generation systems*; Energy Conversion Engineering Conference, 1989. IECEC-89. Proceedings of the 24th Intersociety 08/06/1989 -08/11/1989, 6-11 Aug 1989 Washington, DC, USA; page(s): 2065-2069 vol.4 6-11 Aug 1989.

Ginter, S. Gisler, G. Hanks, J. Havenhill, D. Robinson, W. Spina, L. SatCon Technol. Corp., Tucson, AZ; *Spacecraft energy storage systems:* IEEE Aerospace and Electronics Systems Magazine; page(s): 27-32 Volume: 13, May 1998.

Gosiewski Z., Kulesza Z.: *Wykorzystanie układów FPGA do sterowania siłowników łożyska magnetycznego.*, "Pomiary, Automatyka, Robotyka" R.11, nr 2/2007.

Gully, J.H. Pratap, S.B. Headifen, R.N. Marinos, C. Dick, W. Goodel, B.: *Investigation of an alternator charged pulse forming network with flywheel energy storage* Center for Electromech., Texas Univ., Austin, TX; Magnetics, IEEE Transactions on 04/28/1992 -04/30/1992, 28-30 Apr 1992.

Hall C. D.: *High Speed Flywheels for Integrated Energy Storage and Attitude Control*. Department of Aeronautics and Astronautics Air Force Institute of Technology/ENY Wright-Petterson Air Force Base, Ohio 45433, Sept. 24, 1997.

Hebner R., Beno J., Walls A.: *Flywheel Batteries Come Around Again*, IEEE Spectrum April, 2002.

Kamiński G., Szczypior J., Biernat A., Smak A., Rowiński A., Kowalski W.: *Konstrukcja modelu maszyny do elektromechanicznego magazynowania energii*, Przegląd Elektrotechniczny 6, 2008.

Kamiński G., Szczypior J., Smak A.: *Analiza kształtu zwojów uzwojeń twornika bezrdzeniowego w maszynach do kinetycznych magazynów energii*. Przegląd Elektrotechniczny LXXXI, 10, 2005, str. 7-14.

Kamiński G., Szczypior J., Smak A.: *Analiza uzwojeń tworników bez rdzeni ferromagnetycznych w maszynach kinetycznych magazynów energii*, SME Opole 2005.

Kamiński G., Szczypior J., Smak A.: *Wybrane problemy konstrukcji maszyny bezszczotkowej stosowanej w kinetycznym magazynie energii.* SME Opole 2005.

Kulesza Z., Gosiewski Z.: *An FPGA implementation of the robust controller for the active magnetic bearing system,* 4th International Conference "Mechatronic Systems and Materials, MSM 2008". Abstract book. Bialystok 2008. s. 126.

Kulesza Z., Gosiewski Z.: *An FPGA implementation of the robust controller for the active magnetic bearing system.* "Solid State Phenomena", Vol. 147-149 (2009), s. 399-409.

Mason L.: *Flywheel Power System*, NASA Lewis Research Center, Flywheel Workshop, Oct. 7, 1998.

Mulcahy, T.M. Hull, J.R. Uherka, K.L. Abboud, R.G. Juna, J.J.: *Test results of 2-kWh flywheel using passive PM and HTS bearings,* Argonne Nat. Lab., IL; Applied Superconductivity, IEEE Transactions on 09/17/2000 -09/22/2000, Mar 2001.

Piróg S., Siostrzonek T., Penczek A., Czekoński J.: *Wirujący zasobnik energii z bezszczotkowym silnikiem prądu stałego – wyniki badań laboratoryjnych* VIII Konferencja Naukowa „Sterowanie w Energoelektronice i Napędzie Elektrycznym" SENE'2007 (pod auspicjami European Power Electronics and Drives Association) Pol. Łódzka Łódź 21-23 listopad 2007 (materiały konferencji t. II, str. 379-385..

Piróg S., Siostrzonek T., Penczek A.: *The flywheel energy storage with brushless DC motor* International conference on Power ELectronics and Intelligent Control for Energy Conservation: Warsaw, Poland, October 16–19, 2005.

Piróg S.: *Elektromechaniczne magazyny energii* Napędy i Sterowanie nr. 12 2006, str. 115-132.

Piróg S.: *Magazyny energii* SENE 2007: VIII krajowa konferencja naukowa Sterowanie w Energoelektronice i Napędzie Elektrycznym, Łódź, 21–23 listopada 2007 r.

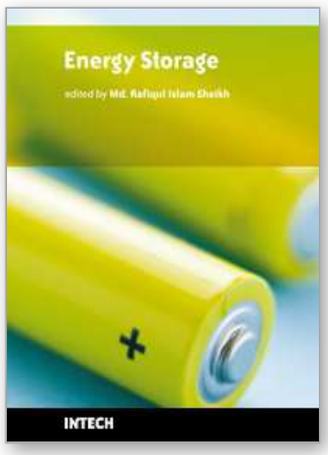


**Energy Storage**

Edited by Rafiqul Islam Sheikh

ISBN 978-953-307-119-0
Hard cover, 142 pages
**Publisher** Sciyo
**Published online** 27, September, 2010
**Published in print edition** September, 2010

Electricity is more versatile in use because it is a highly ordered form of energy that can be converted efficiently into other forms. However, the disadvantage of electricity is that it cannot be easily stored on a large scale. One of the distinctive characteristics of the electric power sector is that the amount of electricity that can be generated is relatively fixed over short periods of time, although demand for electricity fluctuates throughout the day. Almost all electrical energy used today is consumed as it is generated. This poses no hardship in conventional power plants, where the fuel consumption is varied with the load requirements. However, the photovoltaic and wind, being intermittent sources of power, cannot meet the load demand all of the time. Wherever intermittent power sources reach high levels of grid penetration, energy storage becomes one option to provide reliable energy supplies. These devices can help to make renewable energy more smooth and reliable, though the power output cannot be controlled by the grid operators. They can balance micro grids to achieve a good match between generation and load demand, which can further regulate the voltage and frequency. Also, it can significantly improve the load availability, a key requirement for any power system. The energy storage, therefore, is a desired feature to incorporate with renewable power systems, particularly in stand alone power plants. The purpose of this book is twofold. At first, for the interested researcher it shows the importance of different Energy Storage devices, but secondly, and more importantly, it forms a first attempt at dissemination of knowledge to the wider non-expert community who may wish to consider Energy Storage device for specific application. Thus this book will be helpful to provide an indication of the tools necessary for an assessment to be made Energy Storage device more powerful.

**How to reference**

In order to correctly reference this scholarly work, feel free to copy and paste the following:

Tomasz Siostrzonek, Stanisław Piróg and Marcin Baszyński (2010). The High-Speed Flywheel Energy Storage System, Energy Storage, Rafiqul Islam Sheikh (Ed.), ISBN: 978-953-307-119-0, InTech, Available from: http://www.intechopen.com/books/energy-storage/the-high-speed-flywheel-energy-storage-system-

INTECH
open science | open minds

**InTech Europe**
University Campus STeP Ri
Slavka Krautzeka 83/A
51000 Rijeka, Croatia

**InTech China**
Unit 405, Office Block, Hotel Equatorial Shanghai
No.65, Yan An Road (West), Shanghai, 200040, China
中国上海市延安西路65号上海国际贵都大饭店办公楼405单元

Phone: +385 (51) 770 447
Fax: +385 (51) 686 166
www.intechopen.com

Phone: +86-21-62489820
Fax: +86-21-62489821



IntechOpen

IntechOpen